

# Distinct biological activity of Lewy body $\alpha$ -Synuclein strain in mice

Norihito Uemura (✉ [nuemura@kuhp.kyoto-u.ac.jp](mailto:nuemura@kuhp.kyoto-u.ac.jp))

University of Pennsylvania School of Medicine <https://orcid.org/0000-0002-6251-0810>

Nicholas Marotta

University of Pennsylvania School of Medicine

Jahan Ara

University of Pennsylvania School of Medicine

Emily Meymand

University of Pennsylvania School of Medicine

Bin Zhang

University of Pennsylvania

Hiroshi Kameda

Juntendo University Graduate School of Medicine

Masato Koike

Juntendo University <https://orcid.org/0000-0002-3174-5684>

Kelvin Luk

University of Pennsylvania <https://orcid.org/0000-0002-6591-6269>

John Trojanowski

University of Pennsylvania

Virginia Lee

University of Pennsylvania <https://orcid.org/0000-0003-3536-6902>

---

## Article

### Keywords:

**Posted Date:** February 16th, 2023

**DOI:** <https://doi.org/10.21203/rs.3.rs-2579805/v1>

**License:**   This work is licensed under a Creative Commons Attribution 4.0 International License.

[Read Full License](#)

---

# Abstract

Extraction of  $\alpha$ -Synuclein ( $\alpha$ Syn) aggregates from Lewy body disease (LBD) brains has been widely described yet templated fibrillization of LB- $\alpha$ Syn often fails to propagate its structural and functional properties. We recently demonstrated that aggregates amplified from LB- $\alpha$ Syn (ampLB) show distinct biological activities *in vitro* compared to human  $\alpha$ Syn preformed fibrils (hPFF) formed *de novo*. Here we compare the *in vivo* biological activities of hPFF and ampLB regarding seeding activity, latency in inducing pathology, distribution of pathology, inclusion morphology, and cell-type preference. Injection of ampLB into mice expressing only human  $\alpha$ Syn (Thy1:*SNCA/Snca*<sup>-/-</sup> mice) induced pathologies similar to those of LBD subjects that were distinct from those induced by hPFF-injection or developing spontaneously with aging. Importantly,  $\alpha$ Syn aggregates in ampLB-injected Thy1:*SNCA/Snca*<sup>-/-</sup> mice maintained the unique biological and conformational features of original LB- $\alpha$ Syn. These results indicate that ampLB-injection, rather than conventional PFF-injection or  $\alpha$ Syn overexpression, faithfully models key aspects of LBD.

## Introduction

Lewy bodies (LB) are intraneuronal inclusions largely composed of  $\alpha$ -Synuclein ( $\alpha$ Syn) and are found in Lewy body diseases (LBD), a family which encompasses Parkinson's disease (PD), dementia with Lewy bodies (DLB), and Alzheimer's disease (AD) with LB co-pathology<sup>1,2</sup>. Patients with PD first show motor dysfunction (i.e., parkinsonism) but eventually develop cognitive dysfunction, diagnosed as PD with dementia (PDD)<sup>3</sup>. A diagnosis of DLB is given to patients in whom cognitive dysfunction occurs before or concurrently with the motor dysfunction<sup>4</sup>. LB co-pathology is also commonly observed in subjects pathologically diagnosed with AD<sup>2,5</sup>. An additional synucleinopathy is represented by multiple system atrophy (MSA), a clinically distinct entity characterized by the abundance of oligodendroglial  $\alpha$ Syn pathology<sup>6,7</sup>.

$\alpha$ Syn is highly expressed in neurons, existing in an equilibrium of soluble cytosolic and membrane-bound  $\alpha$ -helical forms<sup>8</sup>. However, recombinant  $\alpha$ Syn monomers easily undergo aggregation in physiological buffer conditions and form  $\beta$ -sheet-rich amyloid structures that resemble those observed in LB in diseased brains<sup>9,10</sup>. These  $\alpha$ Syn aggregates generated *de novo* from recombinant  $\alpha$ Syn under controlled conditions (commonly referred to as preformed fibrils; PFF) have been widely used to study different aspects of LBD over the past decade. PFF work as a template to recruit and seed the misfolding of endogenous  $\alpha$ Syn in cultured cells and neurons<sup>11,12</sup>. Similarly, PFF inoculation induces  $\alpha$ Syn inclusions in animal brains, and is accompanied subsequently by intercellular transmission of the  $\alpha$ Syn pathology<sup>13,14</sup>, a phenomenon also inferred from autopsy studies on subjects with PD<sup>15-17</sup>.

Previous studies have demonstrated the presence of distinct  $\alpha$ Syn conformers, or strains, among  $\alpha$ Syn aggregates generated *in vitro* as well as those extracted from synucleinopathy brains, that have different biological activities<sup>18-26</sup>. Cryogenic electron microscopy (Cryo-EM) studies have also revealed atomic-

level structural differences among human  $\alpha$ Syn preformed fibrils (hPFF), LBD  $\alpha$ Syn fibrils, and MSA  $\alpha$ Syn fibrils<sup>27,28</sup>. Based on these observations, it has been hypothesized that the clinical and pathological heterogeneity in synucleinopathies arises from distinct  $\alpha$ Syn strains.

Despite the clear influence of fibril structure on  $\alpha$ Syn *in vitro* and *in vivo* pathological activity with respect to seeding potency, inclusion morphology, cell tropism, and biophysical signatures, attempts to generate recombinant fibrils that faithfully recapitulate the properties of brain-derived  $\alpha$ Syn aggregates have been met with limited success. Furthermore, even though brain-derived  $\alpha$ Syn aggregates can template the fibrillization of recombinant  $\alpha$ Syn, as observed in seeded aggregation assays or protein misfolding cyclic amplification-based strategies using brain lysates or cerebrospinal fluid, fibrils generated in this manner remain conformationally and functionally distinct from brain-derived  $\alpha$ Syn aggregates<sup>27–31</sup>.

Highlighting these differences, we recently demonstrated differences in pathological activity *in vitro* and conformational features between hPFF and  $\alpha$ Syn aggregates extracted from LBD brains (LB- $\alpha$ Syn)<sup>32</sup>. In order to bridge this gap and to overcome the limited availability and low seeding activity of LB- $\alpha$ Syn compared to  $\alpha$ Syn aggregates extracted from MSA brains<sup>20</sup>, we established a method for amplifying LB- $\alpha$ Syn using recombinant human  $\alpha$ Syn monomers. By optimizing the stoichiometry of LB- $\alpha$ Syn and recombinant  $\alpha$ Syn monomers in assembly mixtures, this template-seeded amplification approach successfully replicated the conformational features of original LB- $\alpha$ Syn and unique pathological activity *in vitro*<sup>32</sup>.

Here, we aimed to uncover whether or not the distinct pathological features induced by the LB- $\alpha$ Syn strain are preserved in the brain. Our findings demonstrate conspicuous differences in pathological features induced by hPFF vs ampLB in the brains of wild-type (WT) mice. We then developed a novel LBD mouse model through injection of amplified LB (ampLB) into mice expressing only human  $\alpha$ Syn (Thy1:*SNCA/Snca*<sup>-/-</sup> mice). The comparisons of the ampLB-injected Thy1:*SNCA/Snca*<sup>-/-</sup> mice with LBD subjects, hPFF-injected Thy1:*SNCA/Snca*<sup>-/-</sup> mice, and old Thy1:*SNCA/Snca*<sup>-/-</sup> mice with spontaneous  $\alpha$ Syn pathology further solidify the role of conformation as a determinant of  $\alpha$ Syn pathological activity. Our results provide a novel approach for improving currently available LBD models induced by PFF-injection or  $\alpha$ Syn overexpression.

## Results

### Lewy body amplification increases $\alpha$ Syn pathology induced in WT mice

We previously observed that striatal injection of LB- $\alpha$ Syn only induced sparse  $\alpha$ Syn pathology when injected into WT mouse brains<sup>20</sup>. We therefore sought to augment the level of  $\alpha$ Syn pathology by increasing the amount of LB- $\alpha$ Syn injected and by injecting ampLB (Figure 1A). Our LB- $\alpha$ Syn amplification methodology increases the  $\alpha$ Syn concentration 20 times, up to 200 ng/ $\mu$ l<sup>32</sup>. We injected LB- $\alpha$ Syn at two doses: 50 ng, the same dose as we injected previously<sup>20</sup> or 170 ng, the maximum dose achievable with brain-derived lysate (Table S2). For ampLB-injection, we injected either

100 ng, a comparable quantity to LB- $\alpha$ Syn injection, or 500 ng, the maximum dose we could inject with ampLB. We analyzed  $\alpha$ Syn pathology at 3, 6, and 9 months post-injection (MPI) and quantified the number of phospho-serine129  $\alpha$ Syn (pSyn)-positive neuronal somatic inclusions. Both LB- $\alpha$ Syn and ampLB induced  $\alpha$ Syn pathology in a dose- and time-dependent manner, though the higher concentration (170 ng) of LB- $\alpha$ Syn only induced mild  $\alpha$ Syn pathology throughout the brain (Figures 1B–D). Meanwhile, ampLB induced more  $\alpha$ Syn pathology than LB- $\alpha$ Syn, and 500 ng of ampLB induced the most severe  $\alpha$ Syn pathology (Figures 1B–D). Based on these results, we decided to inject 500 ng of ampLB in mice for most experiments using WT mice.

LB- $\alpha$ Syn only comprises less than 2% of total protein in LBD brain lysates (Tables S2). To examine the effects of contaminants on  $\alpha$ Syn pathogenesis in mouse primary neurons and mouse brains, we immunodepleted  $\alpha$ Syn in LBD brain lysate (Figure 1E). hPFF and immunodepleted brain lysate mixed with hPFF induced neurite-dominant  $\alpha$ Syn pathology, while LB- $\alpha$ Syn and ampLB induced soma-dominant  $\alpha$ Syn pathology in mouse primary neurons (Figure 1F). For mouse brain injection, we used the following materials: hPFF, immunodepleted brain lysate mixed with hPFF (designated as mixed material), original LB- $\alpha$ Syn used to generate ampLB, and ampLB. hPFF- and mixed material-injected WT mice showed similar distribution and amount of  $\alpha$ Syn pathology, while ampLB-injected samples induced significantly higher  $\alpha$ Syn pathology than them at 6MPI (Figure 1G). These results suggest that contaminants contained in LB- $\alpha$ Syn have minimal effects on hPFF-induced  $\alpha$ Syn pathology both *in vitro* and *in vivo*. Moreover, the results also suggest distinct pathological activity between hPFFs and ampLBs in the presence of similar contaminants, further supporting the faithful amplification of LB- $\alpha$ Syn.

### **Distinct biological activity between hPFF and ampLB in WT mice**

To further characterize the pathological activity of ampLB in WT mice, we generated brain lysates from 2 AD cases, 2 PDD cases, and 2 DLB cases, and determined possible differences among ampLB generated from different LBD cases. We then validated ampLB from each brain lysate by testing its ability to induce distinct morphology of  $\alpha$ Syn pathology in mouse primary neurons (Figure S1). We then injected WT mice with 500 ng of ampLB preparations as well as 500 ng and 5  $\mu$ g of hPFF, and analyzed them histologically at 3, 6, and 9MPI (Figure 2A). hPFF-injected samples showed the highest amount of  $\alpha$ Syn pathology in brains at 6MPI. In contrast, all the ampLB-injected samples showed little  $\alpha$ Syn pathology at 3MPI but showed much more pathology at 6MPI, which was further increased at 9MPI (Figures 2B–D). Based on the numbers of neuronal somatic inclusions at 6MPI, ampLB preparations showed 5–50 times more seeding activity than hPFF. Compared with the numbers of neuronal inclusions at 6MPI, hPFF and ampLB preparations induced 60–80% and 5–10% of the inclusions at 3MPI, respectively, suggesting that ampLB take longer to induce  $\alpha$ Syn pathology than hPFF (Figure 2D). The numbers of neuronal inclusions induced by ampLB-injection in the SNpc also jumped at 6MPI but were decreased at 9MPI (Figures S2A and S2B). The numbers of tyrosine hydroxylase (TH)-positive neurons in the ipsilateral SNpc were significantly decreased compared with those in the contralateral SNpc in AD2 and PDD1 ampLB-injected samples at 9MPI (Figure S2C), suggesting that the decrease in numbers of neuronal inclusions was caused by TH-positive neuron loss. Biochemical analysis revealed that injected ampLB, which were



generated from human  $\alpha$ Syn monomers, were almost completely degraded by 3MPI (Figure S3). Meanwhile, mouse  $\alpha$ Syn and pSyn, including their monomeric and oligomeric forms, were increased over time, suggesting that pSyn-positive pathology induced by ampLB-injection was composed of endogenous mouse  $\alpha$ Syn.

Since we observed ~10-fold differences in seeding activity in WT mouse brains among ampLB preparations, we sought to identify the main contributing factors. One of each ampLB preparation generated from AD and PDD brain lysate (AD2 and PDD1) showed high seeding activity, suggesting that the differences in seeding activity were not disease-specific but case-specific. We did not find any clear correlation between seeding activity and age at onset or disease duration (Tables S1 and S2). One factor we found was the total protein in ampLB preparations, which was negatively correlated with the seeding activity both *in vivo* and *in vitro*, albeit not reaching statistical significance (Figures S4A and S4B). The *in vivo* and *in vitro* seeding activity seemed to be positively correlated (Figures S4C).

We next analyzed the distribution of  $\alpha$ Syn pathology in hPFF- and ampLB-injected samples at 6 and 9MPI. hPFF-injected samples showed the most severe pathology in the striatum, the injection site, while all the ampLB-injected samples showed the most severe pathology in some cortical areas and the amygdala (Figures 2E and S5A). We quantitatively measured proportion of pSyn-positive area based on the classification of brain regions shown in Figure S5B. Heatmap and principal component analysis showed the differences in distribution of  $\alpha$ Syn pathology between hPFF- and ampLB-injected samples (Figures 2F, 2G, S5C, and S5D). We further classified brain regions into several brain systems to statistically analyze the differences in distribution of  $\alpha$ Syn pathology induced by hPFF and LBD (including AD, PDD, and DLB) ampLB preparations. The significant differences observed in some brain systems further validated the difference in distribution of  $\alpha$ Syn pathology between hPFF- and ampLB-injected samples (Figures 2H and S5E). Importantly, we did not observe clear differences among LBD (AD, PDD, and DLB) from these analyses.

Next, we examined the morphology of pSyn-positive neuronal inclusions induced by hPFF, ampLB, and LB- $\alpha$ Syn injection. hPFF-injected samples showed various morphology of neuronal inclusions, while ampLB- and LB- $\alpha$ Syn-injected samples mostly showed diffuse somatic pathology (Figures 3A). We classified neuronal inclusions into three types based on their morphology: diffuse somatic pathology (diffuse), isolated compact pathology (compact), and granular pathology (granule) (Figures 3B). The proportion of each morphology seen in hPFF-injected samples were clearly different from those seen in ampLB- and LB- $\alpha$ Syn-injected samples. All the ampLB-injected samples showed mostly diffuse pathology, and the proportion of this pathology was significantly different from that of hPFF-injected samples (Figures 3C). Aside from morphological differences, we found that ~10% of neurons with pSyn-positive somatic inclusions also contained intranuclear inclusions in hPFF-injected mice, while these were rarely observed in ampLB-injected ones (Figures 3D) and further verified by confocal microscopy that a subset of neuronal inclusions in hPFF-injected samples are intranuclear.

Additionally, we found cell-type preference as another difference between hPFF- and ampLB-induced pathology. hPFF induced glial inclusions in WT mouse brains, especially in the corpus callosum, in a dose- and time-dependent manner, the observation we previously reported for mouse  $\alpha$ Syn PFF<sup>33</sup> (Figures 3E and 3F). We further confirmed that these glial inclusions were present in Olig2-positive oligodendroglia, but not in glial fibrillary acidic protein (GFAP)-positive astrocytes or ionized calcium-binding adaptor protein-1 (Iba1)-positive microglia (Figures 3G). Significantly, glial inclusions were rarely observed in all the ampLB-injected samples up to 9 MPI (Figures 3I).

### **Modeling LBD in Thy1:*SNCA*/*Snca*<sup>-/-</sup> mice**

Because of the significant differences in biological activity between hPFF and the LB- $\alpha$ Syn strains in cultured cells and WT mouse brains, we sought to generate a novel LBD animal model that would recapitulate the spread of the LB- $\alpha$ Syn strain in brain. Considering possible differences in pathology induced by human vs mouse  $\alpha$ Syn, we generated mice that only express human  $\alpha$ Syn by crossing mice expressing human  $\alpha$ Syn under a mouse Thy1 promoter (Thy1:*SNCA* mice) with *Snca* knock-out (*Snca*<sup>-/-</sup>) mice (Figure 4A). The resulting Thy1:*SNCA*/*Snca*<sup>-/-</sup> mice expressed high levels of  $\alpha$ Syn compared with WT mice especially in the brainstem, cerebellum, and spinal cord (Figure S6A). However, Thy1:*SNCA*/*Snca*<sup>-/-</sup> mice expressed low levels of  $\alpha$ Syn in the SN, including dopaminergic neurons (data not shown). Western blot analysis showed Thy1:*SNCA*/*Snca*<sup>-/-</sup> mice expressed ~ 4-fold more  $\alpha$ Syn than WT mice in the entire brains (Figure S6B). We injected 1  $\mu$ g of ampLB into the dorsal hippocampus of Thy1:*SNCA*/*Snca*<sup>-/-</sup> mice and conducted pathological analyses at 3, 6, and 9MPI (Figure 4A and S6C). These mice showed severe  $\alpha$ Syn pathology in the ipsilateral ventral dentate gyrus (DG) but only showed little pathology in other brain regions at 3MPI (Figures 4B and 4C). They showed very severe pathology in the ipsilateral hippocampus and severe pathology in some brain regions at 6MPI, with more pathology especially in the brainstem at 9MPI. Although Thy1:*SNCA*/*Snca*<sup>-/-</sup> mouse neurons showed stronger pSyn immunoreactivity than WT mouse neurons, ampLB-induced  $\alpha$ Syn inclusions were clearly distinguished based on their even stronger pSyn staining intensity and morphology. We evaluated pathological changes in the ipsilateral ventral DG because of its remarkable  $\alpha$ Syn pathology during the time course (Figure 4D). The number of NeuN-positive neurons in ampLB injected animals was significantly decreased compared with that of PBS-injected animals from 3MPI, and that was further decreased in a time-dependent manner. Both GFAP- and Iba1-positive areas were significantly increased compared with PBS-injected samples from 3MPI, suggesting reactive astrogliosis and microglial activation.

We conducted behavioral analyses on ampLB-injected Thy1:*SNCA*/*Snca*<sup>-/-</sup> mice together with PBS-injected WT mice and Thy1:*SNCA*/*Snca*<sup>-/-</sup> mice between 6 and 8MPI. The open field test showed longer total distance traveled in Thy1:*SNCA*/*Snca*<sup>-/-</sup> mice than that of PBS-injected WT mice, indicative of their hyperactivity (Figure S6D). The Y maze test showed no significant differences in alternation among the groups (Figure S6E). In the probe trial of the Barnes maze, time spent in target zone was not different between day1 and day10 in PBS-injected Thy1:*SNCA*/*Snca*<sup>-/-</sup> mice, while that was significantly decreased in ampLB-injected Thy1:*SNCA*/*Snca*<sup>-/-</sup> mice at day10 compared with day1 (Figures 4E and

S6F). Likewise, in the cued fear conditioning test, freezing time during auditory cue was not different between day1 and day10 in PBS-injected Thy1:*SNCA/Snca*<sup>-/-</sup> mice, while that was significantly decreased in ampLB-injected Thy1:*SNCA/Snca*<sup>-/-</sup> mice at day10 compared with day1 (Figures 4F and S6G). The time difference between day1 and day10 was significantly decreased in ampLB-injected Thy1:*SNCA/Snca*<sup>-/-</sup> mice compared with PBS-injected Thy1:*SNCA/Snca*<sup>-/-</sup> mice. These results suggest that injection of ampLB into the hippocampus induced impairment of spatial and cued fear memory retention.

### **Pathological and phenotypic features of hPFF-injected Thy1:*SNCA/Snca*<sup>-/-</sup> mice and old Thy1:*SNCA/Snca*<sup>-/-</sup> mice with spontaneous $\alpha$ Syn pathology**

Aside from ampLB-injection, we also applied hPFF-injection to Thy1:*SNCA/Snca*<sup>-/-</sup> mice (Figure 5A). hPFF-injected Thy1:*SNCA/Snca*<sup>-/-</sup> mice showed rapid spread of  $\alpha$ Syn pathology in the brain with very severe pathology in the ipsilateral DG and severe pathology in the brainstem regions at 3MPI, followed by very severe pathology in the ipsilateral DG, brainstem, and spinal cord at 6MPI (Figures 5C and 5D). Mice showed paralysis and ataxia from ~5MPI and did not survive beyond 6MPI (Figure 5B and Movie S1).

We found that some of the old Thy1:*SNCA/Snca*<sup>-/-</sup> mice without ampLB- or hPFF-injection developed spontaneous  $\alpha$ Syn pathology over 13 months of age. We first observed that some Thy1:*SNCA/Snca*<sup>-/-</sup> mice exhibited paralysis and ataxia and then died (Figure 5E). Their motor dysfunction resembled that of hPFF-injected mice. All of the mice showed very severe pathology especially in the brainstem and spinal cord (Figures 5F and 5G). We also sacrificed old asymptomatic Thy1:*SNCA/Snca*<sup>-/-</sup> mice and found less severe pathology in some of them. We classified them into mildly and moderately affected cases based on the severity of  $\alpha$ Syn pathology (Figures 5E–G).

### **Similarities and differences in pathological features among Thy1:*SNCA/Snca*<sup>-/-</sup> mouse models and LBD subjects**

We then evaluated the similarities and differences in pathological features among Thy1:*SNCA/Snca*<sup>-/-</sup> mouse models and LBD subjects. AmpLB-injected Thy1:*SNCA/Snca*<sup>-/-</sup> mice and LBD subjects showed large spheroid-like structures, which were sometimes bigger than small neurons (Figure 6A). These spheroid-like structures were positive for neurofilament, suggesting axonal swellings in addition to cell body inclusions (Figure 6B). Consistent with these observations, pSyn-positive expanded myelinated axons filled with filamentous structures were observed in ampLB-injected Thy1:*SNCA/Snca*<sup>-/-</sup> mice by immunoelectron microscopy (Figure 6C). Meanwhile, hPFF-injected Thy1:*SNCA/Snca*<sup>-/-</sup> mice and old Thy1:*SNCA/Snca*<sup>-/-</sup> mice with spontaneous  $\alpha$ Syn pathology showed neuronal somatic  $\alpha$ Syn inclusions with abundant fine neuritic  $\alpha$ Syn pathology (Figure 6D).

hPFF-injected Thy1:*SNCA/Snca*<sup>-/-</sup> mice and Thy1:*SNCA/Snca*<sup>-/-</sup> mice with spontaneous  $\alpha$ Syn pathology showed dense pSyn-positive inclusions in neuronal soma sometimes with intranuclear inclusions (Figure

6E). The pSyn-positive area in neuronal soma of those mice was larger than that of ampLB-injected Thy1:*SNCA/Snca*<sup>-/-</sup> mice (Figure 6F). We confirmed that at least some of neuronal inclusions contained intranuclear inclusions by confocal microscopy (Figure 6G). We also examined αSyn inclusions in neuronal soma in ampLB- and hPFF-injected Thy1:*SNCA/Snca*<sup>-/-</sup> mice by immunoelectron microscopy. Bundles of pSyn-positive filamentous structures were mostly observed in cytosol in both ampLB- and hPFF-injected Thy1:*SNCA/Snca*<sup>-/-</sup> mice (Figure S7A–C).

### **AmpLB-induced pathological αSyn in Thy1:*SNCA/Snca*<sup>-/-</sup> mice maintains the biological and conformational features of original LB-αSyn**

Finally, we performed biochemical extraction on Thy1:*SNCA/Snca*<sup>-/-</sup> mouse brains to examine the biological and conformational features of αSyn aggregates (Figures 7A and S8A). As expected, little sarkosyl-insoluble αSyn was obtained from the brains of Thy1:*SNCA/Snca*<sup>-/-</sup> mice without spontaneous αSyn pathology (Figure S8B and Table S3). Meanwhile, considerable amount of sarkosyl-insoluble, pSyn-positive αSyn aggregates was obtained from the brains of ampLB- and hPFF-injected Thy1:*SNCA/Snca*<sup>-/-</sup> mice and Thy1:*SNCA/Snca*<sup>-/-</sup> mice with spontaneous αSyn pathology (Figure S8B and Table S3). We first transduced those αSyn aggregates into mouse primary neurons to see their biological activity. αSyn aggregates from Thy1:*SNCA/Snca*<sup>-/-</sup> mice without spontaneous pathology induced little pSyn-positive pathology. However, those from ampLB-injected Thy1:*SNCA/Snca*<sup>-/-</sup> mice induced soma-dominant αSyn pathology, while those from hPFF-injected Thy1:*SNCA/Snca*<sup>-/-</sup> mice and Thy1:*SNCA/Snca*<sup>-/-</sup> mice with spontaneous αSyn pathology induced neurite-dominant αSyn pathology like hPFF (Figure 7B).

In order to determine whether conformational properties of ampLB continued to be propagated *in vivo*, we next conducted partial proteinase K (PK) digestion on αSyn aggregates isolated from Thy1:*SNCA/Snca*<sup>-/-</sup> mouse brains and the original LB-αSyn used for the ampLB-injection. Digestion reactions were stopped at 1, 5, 15, and 30 min. αSyn aggregates from ampLB-injected Thy1:*SNCA/Snca*<sup>-/-</sup> mice and the original LB-αSyn showed similar digestion profiles, which were different from those from hPFF-injected Thy1:*SNCA/Snca*<sup>-/-</sup> mice and Thy1:*SNCA/Snca*<sup>-/-</sup> mice with spontaneous αSyn pathology (Figure 7C). We conducted PK digestion on multiple samples from each group for 15 min and ran them in a single gel. The samples from each group showed similar digestion profiles, and largely reflected the treatment group from which they were derived. Altogether, these results suggest that pathological αSyn aggregates in ampLB-injected Thy1:*SNCA/Snca*<sup>-/-</sup> mice maintained the biological and conformational features of the original LB-αSyn. Moreover, these features are clearly different from those in hPFF-injected Thy1:*SNCA/Snca*<sup>-/-</sup> mice and Thy1:*SNCA/Snca*<sup>-/-</sup> mice with spontaneous αSyn pathology. Interestingly, the pathological αSyn aggregates in hPFF-injected Thy1:*SNCA/Snca*<sup>-/-</sup> mice and Thy1:*SNCA/Snca*<sup>-/-</sup> mice with spontaneous αSyn pathology showed similar biological and conformational features to each other.

## Discussion

Although multiple previous studies have investigated the effect of injecting LBD brain lysates into animal brains, a unique pathological profile induced by LB- $\alpha$ Syn has not been reported thus far<sup>14, 20, 21, 26, 34–36</sup>. This may be partly due to the low  $\alpha$ Syn yield and relatively low seeding activity of LB- $\alpha$ Syn compared with  $\alpha$ Syn extracted from MSA brains. In this study, we described for the first time the detailed biological activity of a prototypic LB- $\alpha$ Syn strain in animal brains by using an amplification methodology which we recently established<sup>32</sup>.

This approach allowed us to compare the pathological features induced by the same doses of hPFF and ampLB. We report here differences in biological activity between hPFF and ampLB in WT mouse brains that are reflected in seeding activity, latency in inducing pathology, distribution of pathology, morphology of neuronal inclusions, and cell-type preference. Meanwhile, we did not observe obvious disease-specific differences in biological activity among ampLB preparations generated from AD, PDD, and DLB brain lysates. These results are consistent with a recent Cryo-EM study showing essentially undistinguishable atomic-level core structures among PD, PDD and DLB  $\alpha$ Syn filaments<sup>28</sup>, and suggest that the differences in clinical and pathological features among these LBD may arise from other factors than strain differences alone. However, we observed case-specific differences of up to  $\sim 10$ -fold in seeding activity in WT mouse brains among ampLB preparations. High seeding activity is important to sufficiently induce  $\alpha$ Syn pathology and model LBD in animals. In this study, we found a negative correlation between seeding activity and total protein or contaminants in ampLB preparations, but further studies are needed to identify the factors affecting seeding activity. Nonetheless, our results showed that seeding activity *in vitro* may help predict the amount of pathology induced in animal brains.

Currently, PFF-injected animals are widely used for modeling and understanding LBD. However, significant differences in biological activity between hPFF and the LB- $\alpha$ Syn strain prompted us towards generating a novel LBD model employing ampLB as a pathological seed in a host that only expresses human  $\alpha$ Syn. AmpLB-injected Thy1:*SNCA/Snca*<sup>-/-</sup> mice recapitulated several characteristics of LBD including the presence of pSyn-positive neuronal inclusions, neuron loss, glial activation, and behavioral abnormalities. As a comparison, we also challenged Thy1:*SNCA/Snca*<sup>-/-</sup> mice with hPFF-injection, which induced rapid spread of  $\alpha$ Syn pathology. Interestingly, we found that some of old Thy1:*SNCA/Snca*<sup>-/-</sup> mice developed  $\alpha$ Syn inclusions without ampLB- or hPFF-injection, which was not reported in the original Thy1:*SNCA* mice<sup>37</sup>. The exacerbation of  $\alpha$ Syn pathology in Thy1:*SNCA/Snca*<sup>-/-</sup> mice compared with Thy1:*SNCA* mice may arise from at least two potential possibilities: (1) differences in genetic background and (2) the absence of endogenous mouse  $\alpha$ Syn expression. The latter is consistent with previous studies showing that deletion of endogenous mouse  $\alpha$ Syn accelerates aggregation of human  $\alpha$ Syn overexpressed in cultured cells and in mice<sup>38, 39</sup>.

We examined the similarities and differences in brain pathological features and biological and conformational features of  $\alpha$ Syn aggregates in brain lysates among the Thy1:*SNCA/Snca*<sup>-/-</sup> mouse

models and LBD subjects. AmpLB-injected Thy1:*SNCA/Snca*<sup>-/-</sup> mice and LBD subjects showed similarities to each other, while they showed clear differences from hPFF-injected Thy1:*SNCA/Snca*<sup>-/-</sup> mice and old Thy1:*SNCA/Snca*<sup>-/-</sup> mice with spontaneous  $\alpha$ Syn pathology. These results have potentially significant implications. First,  $\alpha$ Syn aggregates in ampLB-injected Thy1:*SNCA/Snca*<sup>-/-</sup> mouse brains propagate the biological and conformational features of original LB- $\alpha$ Syn throughout the process of amplification, brain injection, and *in vivo* incubation. This further suggests that the similarities of pathological features between ampLB-injected Thy1:*SNCA/Snca*<sup>-/-</sup> mice and LBD subjects come from their strain similarities. However, we did not observe  $\alpha$ Syn inclusions in ampLB-injected Thy1:*SNCA/Snca*<sup>-/-</sup> mice that morphologically resemble the brainstem LB consisting of a central core and surrounding halo in LBD subjects. Longer incubation times may be needed for such prototypical LB to be developed, or this may be attributed to different pathological responses between mice and humans. The other important implication is that  $\alpha$ Syn aggregates in Thy1:*SNCA/Snca*<sup>-/-</sup> mice with spontaneous  $\alpha$ Syn pathology showed different features from LB- $\alpha$ Syn even though both Thy1:*SNCA/Snca*<sup>-/-</sup> mice and LBD subjects spontaneously develop human  $\alpha$ Syn aggregates. These results suggest that the LB- $\alpha$ Syn strain is not replicated by human  $\alpha$ Syn overexpression in mice. In other words, introduction of the LB- $\alpha$ Syn strain into human  $\alpha$ Syn-expressing mice is required to faithfully recapitulate LBD pathology. Further studies are needed to investigate what factors are required to generate the LB- $\alpha$ Syn strain confirmation in animals and cultured cells expressing human  $\alpha$ Syn.

A limitation of this study is that we indirectly examined conformations of  $\alpha$ Syn aggregates by partial PK digestion. It is important to directly examine the near-atomic core structures of LB- $\alpha$ Syn, ampLB, and  $\alpha$ Syn aggregates in ampLB-injected animals by Cryo-EM in future studies. Furthermore, since previous studies have shown that fibrillization buffer and post-translational modifications may affect conformations of tau filaments<sup>40,41</sup>, there might be room to further optimize LB- $\alpha$ Syn amplification methodology.

In conclusion, we detail the similarities and differences in features of  $\alpha$ Syn brain pathology and pathological  $\alpha$ Syn aggregates among mouse models and LBD subjects, highlighting the ampLB-injection as a novel strategy for improvement upon conventional PFF-injection or  $\alpha$ Syn overexpression animal models. Considering the unique pathological mechanisms induced by the LB- $\alpha$ Syn strain, ampLB-injected animal models will provide new opportunities to identify therapeutic targets, develop diagnostic imaging tools, and test disease-modifying therapies for LBD.

## Declarations

### Data availability

Source data will be shared by the lead contacts upon request. This paper does not report original code. Any additional information needed to reanalyze the data reported in this paper is available from the lead contacts upon request.

## Acknowledgments

We thank M. O'Reilly, K. Hoxha, Y. Liang, C. Durso, C. Li, D. Riddle, R. Dulce, T. Schuck, and S. Leight for their technical assistance. We thank J. Robinson, Dr. C. Peng, Dr. M. X. Henderson, Dr. A. Caputo, Dr. F. Bassil, Dr. M. T. Uemura, Dr. H. Xu, Dr. S. Porta, and Dr. K. Brunden for their expert opinions. We thank members of the Laboratory of Morphology and Image Analysis, Biomedical Research Core Facilities, Juntendo University Graduate School of Medicine for technical assistance with microscopy. This work was supported NIH / NIA U19 Center grant AG062418-01A1 (JQT and VMYL).

## Author contributions

Conceptualization, N.U., J.Q.T., and V.M.Y.L.; Methodology; N.U., N.P.M., J.A., and K.C.L.; Formal Analysis; N.U. and N.P.M.; Investigation, N.U., N.P.M., J.A., E.M. B.Z., H.K., and M.K.; Resources; K.C.L., J.Q.T., and V.M.Y.L.; Writing – Original Draft, N.U.; Writing – Review & Editing, K.C.L., and V.M.Y.L.; Supervision, J.Q.T., and V.M.Y.L.; Funding Acquisition, J.Q.T., and V.M.Y.L.

## Declaration of interests

The authors declare no competing interests.

## References

1. Spillantini, M.G., *et al.* Alpha-synuclein in Lewy bodies. *Nature* **388**, 839-840 (1997).
2. Hamilton, R.L. Lewy bodies in Alzheimer's disease: a neuropathological review of 145 cases using alpha-synuclein immunohistochemistry. *Brain pathology (Zurich, Switzerland)* **10**, 378-384 (2000).
3. Williams-Gray, C.H., *et al.* The CamPaIGN study of Parkinson's disease: 10-year outlook in an incident population-based cohort. *J Neurol Neurosurg Psychiatry* **84**, 1258-1264 (2013).
4. McKeith, I.G., *et al.* Diagnosis and management of dementia with Lewy bodies: Fourth consensus report of the DLB Consortium. *Neurology* **89**, 88-100 (2017).
5. Robinson, J.L., *et al.* Neurodegenerative disease concomitant proteinopathies are prevalent, age-related and APOE4-associated. *Brain* **141**, 2181-2193 (2018).
6. Tu, P.H., *et al.* Glial cytoplasmic inclusions in white matter oligodendrocytes of multiple system atrophy brains contain insoluble alpha-synuclein. *Ann Neurol* **44**, 415-422 (1998).
7. Poewe, W., *et al.* Multiple system atrophy. *Nature reviews. Disease primers* **8**, 56 (2022).
8. Burre, J., Sharma, M. & Sudhof, T.C. alpha-Synuclein assembles into higher-order multimers upon membrane binding to promote SNARE complex formation. *Proc Natl Acad Sci U S A* **111**, E4274-4283 (2014).
9. Conway, K.A., Harper, J.D. & Lansbury, P.T. Accelerated in vitro fibril formation by a mutant alpha-synuclein linked to early-onset Parkinson disease. *Nature medicine* **4**, 1318-1320 (1998).

10. Araki, K., *et al.* Parkinson's disease is a type of amyloidosis featuring accumulation of amyloid fibrils of  $\alpha$ -synuclein. *Proc Natl Acad Sci U S A* **116**, 17963-17969 (2019).
11. Luk, K.C., *et al.* Exogenous alpha-synuclein fibrils seed the formation of Lewy body-like intracellular inclusions in cultured cells. *Proc Natl Acad Sci U S A* **106**, 20051-20056 (2009).
12. Volpicelli-Daley, L.A., *et al.* Exogenous alpha-synuclein fibrils induce Lewy body pathology leading to synaptic dysfunction and neuron death. *Neuron* **72**, 57-71 (2011).
13. Luk, K.C., *et al.* Pathological alpha-synuclein transmission initiates Parkinson-like neurodegeneration in nontransgenic mice. *Science* **338**, 949-953 (2012).
14. Masuda-Suzukake, M., *et al.* Prion-like spreading of pathological alpha-synuclein in brain. *Brain* **136**, 1128-1138 (2013).
15. Braak, H., *et al.* Staging of brain pathology related to sporadic Parkinson's disease. *Neurobiology of aging* **24**, 197-211 (2003).
16. Li, J.Y., *et al.* Lewy bodies in grafted neurons in subjects with Parkinson's disease suggest host-to-graft disease propagation. *Nature medicine* **14**, 501-503 (2008).
17. Kordower, J.H., Chu, Y., Hauser, R.A., Freeman, T.B. & Olanow, C.W. Lewy body-like pathology in long-term embryonic nigral transplants in Parkinson's disease. *Nature medicine* **14**, 504-506 (2008).
18. Guo, J.L., *et al.* Distinct alpha-synuclein strains differentially promote tau inclusions in neurons. *Cell* **154**, 103-117 (2013).
19. Peelaerts, W., *et al.* alpha-Synuclein strains cause distinct synucleinopathies after local and systemic administration. *Nature* **522**, 340-344 (2015).
20. Peng, C., *et al.* Cellular milieu imparts distinct pathological alpha-synuclein strains in alpha-synucleinopathies. *Nature* **557**, 558-563 (2018).
21. Van der Perren, A., *et al.* The structural differences between patient-derived  $\alpha$ -synuclein strains dictate characteristics of Parkinson's disease, multiple system atrophy and dementia with Lewy bodies. *Acta neuropathologica* **139**, 977-1000 (2020).
22. Lau, A., *et al.* alpha-Synuclein strains target distinct brain regions and cell types. *Nature neuroscience* **23**, 21-31 (2020).
23. Shahnawaz, M., *et al.* Discriminating alpha-synuclein strains in Parkinson's disease and multiple system atrophy. *Nature* **578**, 273-277 (2020).
24. Suzuki, G., *et al.*  $\alpha$ -synuclein strains that cause distinct pathologies differentially inhibit proteasome. *eLife* **9** (2020).
25. Tanudjojo, B., *et al.* Phenotypic manifestation of  $\alpha$ -synuclein strains derived from Parkinson's disease and multiple system atrophy in human dopaminergic neurons. *Nat Commun* **12**, 3817 (2021).
26. Prusiner, S.B., *et al.* Evidence for alpha-synuclein prions causing multiple system atrophy in humans with parkinsonism. *Proc Natl Acad Sci U S A* **112**, E5308-5317 (2015).
27. Schweighauser, M., *et al.* Structures of  $\alpha$ -synuclein filaments from multiple system atrophy. *Nature* **585**, 464-469 (2020).



28. Yang, Y., *et al.* Structures of  $\alpha$ -synuclein filaments from human brains with Lewy pathology. *Nature* **610**, 791-795 (2022).
29. Burger, D., Fenyi, A., Bousset, L., Stahlberg, H. & Melki, R. Cryo-EM structure of alpha-synuclein fibrils amplified by PMCA from PD and MSA patient brains. *bioRxiv*, 2021.2007.2008.451588 (2021).
30. Lövestam, S., *et al.* Seeded assembly in vitro does not replicate the structures of  $\alpha$ -synuclein filaments from multiple system atrophy. *FEBS open bio* **11**, 999-1013 (2021).
31. Sokratian, A., *et al.* Structural and functional landscape of  $\alpha$ -synuclein fibril conformations amplified from cerebrospinal fluid. *bioRxiv*, 2022.2007.2013.499896 (2022).
32. Marotta, N.P., *et al.* Alpha-synuclein from patient Lewy bodies exhibits distinct pathological activity that can be propagated in vitro. *Acta neuropathologica communications* **9**, 188 (2021).
33. Uemura, N., *et al.* Slow Progressive Accumulation of Oligodendroglial Alpha-Synuclein (alpha-Syn) Pathology in Synthetic alpha-Syn Fibril-Induced Mouse Models of Synucleinopathy. *Journal of neuropathology and experimental neurology* **78**, 877-890 (2019).
34. Recasens, A., *et al.* Lewy body extracts from Parkinson disease brains trigger alpha-synuclein pathology and neurodegeneration in mice and monkeys. *Ann Neurol* **75**, 351-362 (2014).
35. Bourdenx, M., *et al.* Identification of distinct pathological signatures induced by patient-derived  $\alpha$ -synuclein structures in nonhuman primates. *Science advances* **6**, eaaz9165 (2020).
36. Arotcarena, M.L., *et al.* Bidirectional gut-to-brain and brain-to-gut propagation of synucleinopathy in non-human primates. *Brain* **143**, 1462-1475 (2020).
37. Rockenstein, E., *et al.* Differential neuropathological alterations in transgenic mice expressing alpha-synuclein from the platelet-derived growth factor and Thy-1 promoters. *Journal of neuroscience research* **68**, 568-578 (2002).
38. Cabin, D.E., *et al.* Exacerbated synucleinopathy in mice expressing A53T SNCA on a Snca null background. *Neurobiology of aging* **26**, 25-35 (2005).
39. Fares, M.B., *et al.* Induction of de novo  $\alpha$ -synuclein fibrillization in a neuronal model for Parkinson's disease. *Proc Natl Acad Sci U S A* **113**, E912-921 (2016).
40. Lövestam, S., *et al.* Assembly of recombinant tau into filaments identical to those of Alzheimer's disease and chronic traumatic encephalopathy. *eLife* **11** (2022).
41. Arakhamia, T., *et al.* Posttranslational Modifications Mediate the Structural Diversity of Tauopathy Strains. *Cell* **184**, 6207-6210 (2021).
42. Toledo, J.B., *et al.* A platform for discovery: The University of Pennsylvania Integrated Neurodegenerative Disease Biobank. *Alzheimer's & dementia : the journal of the Alzheimer's Association* **10**, 477-484.e471 (2014).
43. Volpicelli-Daley, L.A., Luk, K.C. & Lee, V.M. Addition of exogenous  $\alpha$ -synuclein preformed fibrils to primary neuronal cultures to seed recruitment of endogenous  $\alpha$ -synuclein to Lewy body and Lewy neurite-like aggregates. *Nature protocols* **9**, 2135-2146 (2014).

44. McKeith, I.G., *et al.* Diagnosis and management of dementia with Lewy bodies: third report of the DLB Consortium. *Neurology* **65**, 1863-1872 (2005).
45. Bankhead, P., *et al.* QuPath: Open source software for digital pathology image analysis. *Scientific reports* **7**, 16878 (2017).
46. Kameda, H., *et al.* Parvalbumin-producing cortical interneurons receive inhibitory inputs on proximal portions and cortical excitatory inputs on distal dendrites. *The European journal of neuroscience* **35**, 838-854 (2012).

## Online Methods

### Mice

Female C57BL/6 C3H (B6C3) mice at 2 months of age purchased from Charles River were used for the experiments in Figures 1–3. Thy1:*SNCA/Snca*<sup>-/-</sup> mice were generated in the Center for Neurodegenerative Disease Research (CNDR) by crossing Thy1:*SNCA* mouse line 61<sup>37</sup> on a DBA background with *Snca*<sup>-/-</sup> mice on a B6C3 background. Because the transgene is inserted in the X chromosome, only male Thy1:*SNCA/Snca*<sup>-/-</sup> mice were used for this study. To generate male Thy1:*SNCA/Snca*<sup>-/-</sup> mice, female Thy1:*SNCA/Snca*<sup>-/-</sup> mice were crossed with male *Snca*<sup>-/-</sup> mice. Male Thy1:*SNCA/Snca*<sup>-/-</sup> mice and male B6C3 mice as WT mice at 2–3 months of age were used for the experiments in Figures 4–7. Mice were housed in a temperature-controlled room under a 12-hour light/dark cycle with free access to food and water. All animal procedures were approved by the University of Pennsylvania Institutional Animal Care and Use Committee and conformed to the National Institute of Health Guide for Care and Use of Laboratory Animals.

### Primary Hippocampal Neuron Cultures

Primary mouse neurons were prepared from the hippocampus of embryonic day E16–E18 CD1 mouse embryos as described previously<sup>12</sup>. Dissociated hippocampal neurons were plated at 100,000 cells/well (24-well plate) or 17,500 cells/well (96-well plate) in neuron media (Neurobasal medium, Thermo Fisher #21103049) supplemented with B27 (Thermo Fisher #17504044), 2 mM GlutaMax (Thermo Fisher #35050061), and 100 U/ml penicillin/streptomycin (Thermo Fisher #15140122).

### Human patient samples

Detailed clinical characteristics (disease duration, age at death, site of onset, etc.) were ascertained from an integrated neurodegenerative disease database in CNDR at the University of Pennsylvania. Frozen and paraffinized postmortem brain samples were obtained from patient brain donors who underwent autopsy at CNDR between 2002 and 2018. More details on these patients are found in Table S1. All procedures were performed in accordance with local institutional review board guidelines. Written informed consent for autopsy and analysis of tissue sample data was obtained either from patients themselves or their next of kin.

## Biochemical extraction of sarkosyl-insoluble $\alpha$ Syn from human and mouse brains

Biochemical brain extraction was conducted as described previously with minor modifications<sup>32</sup>. All human brain tissues were obtained from the CNDR brain bank<sup>42</sup>. Frontal cortex tissues with a high burden of  $\alpha$ Syn pathology from patients with AD, PDD, and DLB were identified by postmortem neuropathological examination<sup>5</sup>. Biochemical extraction of human brains was performed as described previously<sup>32</sup>. In brief, 5–10 g of frontal cortical gray matter was homogenized in five volumes (w/v) of 1% (v/v) Triton X-100-containing high-salt (HS) buffer (50 mM Tris-HCl pH 7.4, 750 mM NaCl, 10 mM NaF, 5 mM ethylenediaminetetraacetic acid [EDTA]) with protease and protein phosphatase inhibitors, incubated on ice for 20 min, and centrifuged at 180,000  $\times$  g for 30 min. The pellets were then re-extracted with five volumes of 1% (v/v) Triton X-100-containing HS buffer, followed by sequential extraction with five volumes of HS buffer with 30% (w/v) sucrose for myelin floatation. The pellets were then re-suspended and homogenized in 2% (w/v) sarkosyl-containing HS buffer, rotated at room temperature for 1 h or at 4 °C overnight and centrifuged at 180,000  $\times$  g for 30 min. The resulting sarkosyl-insoluble pellets were washed once with Dulbecco's PBS (DPBS, Corning #21-031-CV) and re-suspended in DPBS by sonication (QSonica Microson XL-2000; 60 pulses, setting 2, 0.5 s per pulse). This suspension termed the "sarkosyl-insoluble fraction" or "brain lysate" contained pathological  $\alpha$ Syn referred to as "LB- $\alpha$ Syn" and was used for the experiments. Mouse brain extraction was performed with the same protocol for human brain extraction except that only one round of extraction with 1% Triton X-100-containing HS buffer was performed (Figure S8A). The Triton X-100-soluble fraction was used for the experiments in Figure S6B. The concentrations of  $\alpha$ Syn in the sarkosyl-insoluble fractions were determined by sandwich ELISA (see 'Sandwich ELISA'), and the protein concentrations were examined by bicinchoninic acid (BCA) assay (Tables S2 and S3).

### Sandwich ELISA

Sandwich ELISA was conducted as described previously<sup>32</sup>. To measure the concentration of  $\alpha$ Syn in brain lysates, 384-well Nunc Maxisorp clear plates were coated with 100 ng (30  $\mu$ l per well) of an anti-human  $\alpha$ Syn antibody Syn9027 (CNDR) in sodium carbonate buffer, pH 9.6 and incubated overnight at 4 °C. The plates were washed 4 times with PBS containing 1% (v/v) Tween 20 (PBS-T), and blocked using Block Ace solution (AbD Serotec) overnight at 4 °C. Brain lysates were sonicated with a Diagenode Biorupter sonicator (20 min, 30 s on, 30 s off, 10 °C, high setting), serially diluted in PBS and added to each well. The plates were incubated overnight at 4 °C. The recombinant human  $\alpha$ Syn monomer and hPFF were used as standards. The plates were then washed with PBS-T and an anti-human  $\alpha$ Syn antibody MJFR1 (Abcam #ab138501, 1:1000) or an anti-human  $\alpha$ Syn antibody HuA (CNDR, 1:2000) was added to each well and incubated at 4 °C overnight. After washing, a secondary antibody conjugated with horse radish peroxidase (Cell Signaling Technology #7074, 1:10000) was added to the plates followed by incubation for 1 hr at 37 °C. Following another wash, the plates were developed for 10–15 min using 1-Step Ultra TMB-ELISA substrate solution (Thermo Fisher Scientific #37574, 30  $\mu$ l per well), the reaction

was quenched using 10% phosphoric acid and plates were read at 450 nm on a Molecular Devices Spectramax M5 plate reader.

### **Recombinant $\alpha$ Syn purification and *in vitro* PFF generation**

Purification of recombinant human  $\alpha$ Syn and generation of hPFF was conducted as described previously<sup>43</sup>. The pRK172 plasmid containing a full-length human  $\alpha$ Syn gene was transformed into BL21 (DE3) RIL-competent E. coli (Agilent Technologies #230245). A single colony from the transformed bacteria was expanded in Terrific Broth (12 g/l of Bacto-tryptone, 24 g/l of yeast extract 4% (v/v) glycerol, 17 mM  $\text{KH}_2\text{PO}_4$  and 72 mM  $\text{K}_2\text{HPO}_4$ ) with ampicillin. Bacterial pellets from the growth were sonicated, and the sample was boiled to precipitate undesired proteins. The supernatant was dialyzed with 10 mM Tris, pH 7.6, 50 mM NaCl, 1 mM EDTA overnight. Protein was filtered with a 0.22  $\mu\text{m}$  filter and concentrated using Amicon Ultra-15 centrifugal filters (Millipore Sigma #UFC901008). Protein was then loaded onto a Superdex 200 column and 1 ml fractions were collected. Fractions were run on sodium dodecyl sulfate polyacrylamide gel electrophoresis (SDS-PAGE) and stained with Coomassie blue to select fractions that were highly enriched in  $\alpha$ Syn. These fractions were combined and dialyzed in 10 mM Tris, pH 7.6, 50 mM NaCl, 1 mM EDTA overnight. Dialyzed fractions were applied to a HiTrap Q HP anion-exchange column (GE Healthcare #17115301) and run using a linear gradient from 25 mM NaCl to 1 M NaCl. Collected fractions were run on SDS-PAGE and stained with Coomassie blue. Fractions that were highly enriched in  $\alpha$ Syn were collected and dialyzed with DPBS. Protein was filtered through a 0.22  $\mu\text{m}$  filter and concentrated to 5 mg/ml ( $\alpha$ Syn) with Amicon Ultra-15 centrifugal filters.  $\alpha$ Syn monomer was aliquoted and frozen at  $-80^\circ\text{C}$ . For preparation of PFF,  $\alpha$ Syn monomer was shaken at 1,000 rpm for 7 d. Conversion to PFF was validated by sedimentation at 100,000  $\times$  g for 60 min and by Thioflavin S staining.

### ***In vitro* amplification of LB- $\alpha$ Syn from brain lysates**

LB- $\alpha$ Syn amplification was performed as described previously with minor modifications<sup>32</sup>. LB- $\alpha$ Syn from brain lysates of patients pathologically confirmed with AD, PDD, or DLB was sonicated with a Diagenode Biorupter sonicator (20 min, 30 s on, 30 s off, 10  $^\circ\text{C}$ , high setting). The amplification reaction was set up with 5% LB- $\alpha$ Syn (calculated based on sandwich ELISA), 95% human  $\alpha$ Syn monomer, and DPBS (pH 7.4, without  $\text{Mg}^{2+}$  and  $\text{Ca}^{2+}$ ) at the final  $\alpha$ Syn concentration of 200 or 400 ng/ $\mu\text{l}$ . The solution was incubated at 37  $^\circ\text{C}$  with constant agitation at 1,000 rpm for 14 d. The resulting material (ampLB) was transduced into mouse primary hippocampal neurons to verify the success of amplification of LB- $\alpha$ Syn.

### **$\alpha$ Syn transduction into mouse primary neurons**

$\alpha$ Syn transduction into mouse primary hippocampal neurons was performed as described previously<sup>32</sup>. hPFF, LB- $\alpha$ Syn, ampLB, and  $\alpha$ Syn aggregates extracted from Thy1:*SNCA*/*Snca*<sup>-/-</sup> mouse brains were diluted in DPBS and sonicated with a Diagenode Biorupter sonicator (20 min, 30 s on, 30 s off, 10  $^\circ\text{C}$ , high setting). Neurons were then treated with noted dose of the  $\alpha$ Syn preparations at 7 d *in vitro* (DIV), fixed and immunostained at 14 d post-treatment (21 DIV). The amount of  $\alpha$ Syn transduced in Figures 1F, S1,

and S6C was 25 ng/well. For the treatment with  $\alpha$ Syn aggregates extracted from Thy1:*SNCA/Snca*<sup>-/-</sup> mouse brains in Figure 7B, the brain lysates containing 25 ng of  $\alpha$ Syn or up to 6.4  $\mu$ g of total protein per well were transduced to avoid significant toxicity of contaminants for cultured neurons<sup>32</sup>. The resulting amounts of  $\alpha$ Syn were 2.4 ng/well (Thy1:*SNCA/Snca*<sup>-/-</sup> mice without  $\alpha$ Syn pathology), 19 ng/well (ampLB-injected Thy1:*SNCA/Snca*<sup>-/-</sup> mice), and 25 ng/well (hPFF-injected Thy1:*SNCA/Snca*<sup>-/-</sup> mice and Thy1:*SNCA/Snca*<sup>-/-</sup> mice with spontaneous  $\alpha$ Syn pathology).

### Immunocytochemistry and quantification of neuron pathology

Immunocytochemistry and quantification of pSyn-positive neuronal pathology was performed as described previously<sup>32</sup>. Mouse primary neurons cultured in 96 wells were washed with PBS once and fixed at DIV 21 with 4% (w/v) PFA, 4% (w/v) sucrose, and 1% (v/v) Triton X-100 in PBS. After PBS washes, cells were blocked with 3% (w/v) bovine serum albumin (BSA), 5% (w/v) fetal bovine serum in DPBS for 1 h at room temperature, then incubated with an anti-pSyn antibody 81A (CNRD, 1:5000) and an anti-microtubule associated protein 2 (MAP2) antibody #17028 (CNRD, 1:3000) at 4 °C overnight. The cells were washed 5 times with PBS and incubated with secondary antibodies conjugated with Alexa fluor 488 or 594 (Molecular Probes, 1:1000) for 2 h at room temperature. After washing with PBS, the cells were incubated in DAPI solution (ThermoFisher #D21490, 1:10,000 in PBS) after staining with secondary antibodies and the plates were sealed with adhesive covers. The 96 well plates were scanned with an In Cell Analyzer 2200 (GE Healthcare) with a 10 × or 40 × objective and analyzed using the accompanying software (In Cell Toolbox Analyzer). Quantitation of total 81A signal and the amount of somatic 81A signal was calculated using Cell Profiler ver. 3.1.9 (The Broad Institute). The fraction of somatic inclusions was calculated as the 81A signal intensity (density times area) of somatic objects divided by the total 81A signal intensity. Data are reported as the average of 3 replicate wells for each treatment sample.

### Western blotting

Protein concentrations of samples were determined with a BCA assay kit (Fisher #23223 and 23224) using BSA as a standard (Thermo Fisher #23210). Samples were normalized for total protein content and boiled with SDS-sample buffer for 10 min. Samples (10  $\mu$ g total protein) were separated on 12.5% SDS-polyacrylamide gels and transferred onto 0.2  $\mu$ m nitrocellulose membranes. For the samples digested by PK, NuPAGE Novex 12% Bis-Tris gels (Invitrogen) were used. The membranes were fixed with 4% (w/v) paraformaldehyde in tris buffered saline (TBS) for 30 min to prevent detachment of  $\alpha$ Syn from the blotted membranes. Ponceau staining was performed to visualize the protein transferred to the membranes. After blocked in 5% (w/v) non-fat milk in TBS for 30 min, the membranes were probed at 4 °C overnight with following primary antibodies: an anti-human  $\alpha$ Syn antibody HuA (CNRD, 1:500–3000), an anti-pSyn antibody 81A (CNRD, 1:5000), an anti-human  $\alpha$ Syn-specific antibody LB509 (CNRD, 1:100), an anti-mouse  $\alpha$ Syn-specific antibody D37A6 (Cell signaling #4179, 1:1000), an anti- $\alpha$ Syn antibody Syn1 (BD transduction #610787, 1:500–1000), and an anti-pSyn antibody EP1536Y (abcam #ab51253, 1:5000). Primary antibodies were detected using IRDye 800 (Li-Cor #925-32210) and IRDye 680 (Li-Cor

#925-68071) labeled secondary antibodies, scanned on a Li-Cor Odyssey Imaging System and analyzed using Image Studio software (Li-Cor Biosciences). Densitometric analyses were performed using ImageJ (NIH).

### **Immunodepletion of $\alpha$ Syn from brain lysate**

An anti-human  $\alpha$ Syn monoclonal antibody 9027 was covalently conjugated to Dynabeads M-280, tosylactivated (Invitrogen #14204) per the manufacturer's instructions. Immunodepletion of  $\alpha$ Syn was performed by incubating diluted AD1 brain lysate (10 ng/ $\mu$ l of  $\alpha$ Syn, 50  $\mu$ l total dose) with anti- $\alpha$ Syn antibody-bead complexes containing 68  $\mu$ g of the antibody at 37 °C for 1 h with constant rotation. The immunodepleted fraction was separated from the antibody-bead complex using a magnet. Mock immunodepletion was performed using the equal amount of a control mouse IgG antibody (Jackson Immuno Research). The brain lysate immunodepleted with the anti- $\alpha$ Syn antibody and the control antibody were used for western blot analysis. The  $\alpha$ Syn-depleted brain lysate (2.5  $\mu$ l) mixed with hPFFs (500 ng) was used for mouse brain injection. Diluted AD1 brain lysate (10 ng/ $\mu$ l of  $\alpha$ Syn, 2.5  $\mu$ l total dose) and amplified LB- $\alpha$ Syn generated from AD1 brain lysate (200 ng/ $\mu$ l of  $\alpha$ Syn, 2.5  $\mu$ l total dose) were used for injection as comparisons. Those three injection materials contained almost the same contaminants.

### **Partial PK digestion of $\alpha$ Syn aggregates in brain lysate**

Sarkosyl-insoluble fractions from LBD brains and Thy1:*SNCA/Snca*<sup>-/-</sup> mouse brains were prepared by biochemical brain extraction. For partial PK digestion, 50 ng of  $\alpha$ Syn from each sample was sonicated with a Diagenode Biorupter sonicator (20 min, 30 s on, 30 s off, 10 °C, high setting) and mixed with 0.2  $\mu$ g of PK in DPBS to a final volume of 50  $\mu$ l and incubated at 37 °C for 1, 5, 15, and 30 min. The reaction was stopped with 1 mM PMSF. The samples were boiled with SDS-sample buffer for 10 min and resolved on NuPAGE Novex 12% Bis-Tris gels (Invitrogen). Transferred nitrocellulose membranes were probed with an anti-human  $\alpha$ Syn antibody HuA (CNDR, 1:500) and an anti- $\alpha$ Syn antibody Syn1 (BD transduction #610787, 1:500).

### **Stereotaxic inoculation of mouse brains**

Stereotaxic surgery was performed as described previously with minor modifications<sup>13</sup>. Mice anesthetized with ketamine-xylazine-acepromazine underwent stereotaxic injection. A 30-gauge syringe was used for brain lysate injection, and a 33-gauge syringe was used for hPFF- and ampLB-injection. For pathological analysis in Figures 1–3, WT mice received a unilateral injection of 2.5  $\mu$ l of hPFF (200 ng/ $\mu$ l or 2  $\mu$ g/ $\mu$ l of  $\alpha$ Syn, 500 ng or 5  $\mu$ g total dose) or ampLB (200 ng/ $\mu$ l of  $\alpha$ Syn, 500 ng total dose) into the dorsal striatum (coordinates: 0.2 mm relative to bregma; 2.0 mm from midline; –3.2 mm beneath the skull surface). For biochemical analysis in Figure S3, WT mice received a bilateral injection of 2.5  $\mu$ l of ampLB (400 ng/ $\mu$ l of  $\alpha$ Syn, 1  $\mu$ g total dose) into the dorsal striatum. For pathological, behavioral, and biochemical analysis in Figures 4–7, Thy1:*SNCA/Snca*<sup>-/-</sup> and WT mice received a unilateral injection of 2.5  $\mu$ l of hPFF (400 ng/ $\mu$ l of  $\alpha$ Syn, 1  $\mu$ g total dose), ampLB (400 ng/ $\mu$ l of  $\alpha$ Syn, 1  $\mu$ g total dose), or PBS

into the dorsal hippocampus (coordinates: -2.5 mm relative to bregma; 2.0 mm from midline; -2.4 mm beneath the skull surface). The mice were sacrificed at indicated timepoints and were subjected to histological and biochemical analyses.

### **Immunohistochemical analysis of injected mouse brains**

Mice were deeply anesthetized with ketamine-xylazine-acepromazine. Following intracardial perfusion with PBS, mice were perfused with 15 ml of fixative containing 4% (w/v) PFA in PBS. The brains were collected and immersed in 4% (w/v) PFA in PBS at 4 °C overnight. The brains were embedded in paraffin and then sectioned with a thickness of 6 µm. For immunohistochemical analyses, the sections were incubated at 4°C for 2 d with following primary antibodies: an anti-pSyn antibody EP1536Y (Abcam #ab51253, 1:20000), an anti-TH antibody (Sigma-Aldrich #T2928, 1:10000), an anti-NeuN antibody (Sigma-Aldrich #MAB377, 1:2000), an anti-GFAP antibody 2.2B10 (CNDP, 1:5000), and an anti-Iba1 antibody (Wako #019-19741, 1:2000). Biotinylated secondary antibodies (Vector laboratories) were used for generating diaminobenzidine reaction product, and nuclei were counterstained with hematoxylin.

To quantify the amount of αSyn pathology, every 20<sup>th</sup> paraffin section throughout the brains was stained with an anti-pSyn antibody EP1536Y, and pSyn-positive neuronal somatic inclusions with visible nuclei were manually counted. To assess distribution and severity of αSyn pathology, semi-quantitative analyses were performed for pSyn-positive pathology on the five coronal sections (2.80, 0.26, -1.58, -2.92, and -4.04 mm relative to bregma), and color coded onto heat maps (Figures 1C, 1G, 2E, 4C, 5D, 5G, and S5A). The extent of αSyn pathology was graded as 0–3 (0, no pathology; 0.5, mild; 1, moderate; 2, severe; 3, very severe) based on the criteria described previously<sup>44</sup>, and averaged across samples for each brain region. To quantitatively assess distribution of pSyn-positive area, each brain region shown in Figure S5B was measured using QuPath software<sup>45</sup>. The proportion of pSyn-positive area was averaged across samples for each brain region, and color coded onto heat maps (Figures 2F and S5C). Primary component analysis of distribution of pSyn-positive pathology was performed using GraphPad Prism Software, Version 9.

To assess dopaminergic neuron loss in the SNpc, every 20<sup>th</sup> section was stained with an anti-TH antibody throughout the SNpc. The numbers of TH-positive cells with visible nuclei were manually counted. To assess neuron loss and glial activation in the ventral DG, sections at -3.52 mm relative to bregma were stained with anti-NeuN, GFAP, and Iba1 antibodies. The numbers of NeuN-positive neurons were automatically counted and the GFAP- and Iba1-positive area was measured using QuPath software. Sections were examined with a BX43 microscope (Olympus) or a Panoramic 250 (3DHISTECH) scanner.

For immunofluorescence, the sections were incubated at 4°C for 2 d with following primary antibodies: an anti-pSyn antibody EP1536Y (Abcam #ab51253, 1:5000), an anti-pSyn antibody 81A (CNDP, 1:2000), an anti-pSyn antibody #64 (Wako #015-25191, 1:2000), anti-TH antibody (Sigma-Aldrich #T2928, 1:2000), an anti-Olig2 antibody (Millipore #AB9610, 1:500), an anti-GFAP antibody 2.2B10 (CNDP, 1:2000), an anti-Iba1 antibody (Wako #019-19741, 1:1000), and an anti-phosphorylated neurofilament antibody TA51

(CNDP, 1:500). Fluorescent dye-conjugated secondary antibodies (Vector laboratories) were used, and nuclei were stained with DAPI. Sections were examined with an Eclipse Ni microscope (Nikon) or a TCS SP8 WLL Confocal with STED 3X (Leica).

### **Immunoelectron microscopy**

Preparative procedures for pre-embedding immunoelectron microscopy have been described in detail elsewhere<sup>46</sup>. Mice were deeply anesthetized with ketamine–xylazine–acepromazine. Following intracardial perfusion with 0.1 M phosphate buffer (PB) (pH 7.2), mice were perfused with 30 ml of fixative containing 4% (w/v) PFA and 0.05% (w/v) glutaraldehyde in 0.1 M PB. The brains were removed from the skull immediately after perfusion, post-fixed in 4% (w/v) PFA overnight at 4 °C and coronally sectioned at 50 µm by a vibratome (VT1200S; Leica). Sections were pre-incubated for 30 min in PBS containing 20% (v/v) normal donkey serum (Jackson ImmunoResearch Laboratories), 0.3% (v/v) Photo-flo 600 (Kodak), incubated overnight at 4 °C with 13 µg/ml anti-pSyn rabbit antibody EP1536Y (Abcam #ab51253) in PBS containing 2% (v/v) normal donkey serum and 0.3% (v/v) Photo-flo 600, and then washed twice with PBS. Subsequently, after incubation overnight at 4 °C with 1/100-diluted gold-conjugated anti-rabbit IgG goat antibody (Ultra-small Gold Reagent) in PBS containing 2% (v/v) normal donkey serum and 0.3% (v/v) Photo-flo 600, the sections were post-fixed with 1% (w/v) glutaraldehyde in 0.1 M PB for 10 min. After washes with distilled water, gold particles were developed with a silver enhancement kit (R-GENT SE-EM). The sections were then washed with 0.1 M PB, placed for 40 min in 0.1 M PB containing 1% (w/v) osmium tetroxide, counterstained for 30 min with 1% (w/v) uranyl acetate, dehydrated, and flat-embedded in epoxy resin (Luveak 812; Nacalai Tesque). After polymerization of the resin, approximately 70-nm-thick ultrathin sections were cut with an ultramicrotome (UC6; Leica), stained briefly with 1% (w/v) uranyl acetate and 1% (w/v) lead citrate, and observed with an electron microscope (HT7700; Hitachi).

### **Behavioral analysis**

WT mice injected with PBS, Thy1:*SNCA/Snca*<sup>-/-</sup> mice injected with PBS, and Thy1:*SNCA/Snca*<sup>-/-</sup> mice injected with ampLB were subjected to behavioral tests from 6 to 8MPI. Before every test, the mice were habituated to the experimental environment for more than 30 min. Samples that encountered technical problems were removed from the analyses.

#### *Open field*

Mice were placed at the center of the field inside an open field apparatus (36 × 36 cm) and allowed to move freely for 15 min. The distance traveled and time spent in the center area (18 × 18 cm) were recorded using video tracking software EthoVision XT 15 (Noldus).

#### *Y-maze*



Mice were placed at the end of one arm of the Y-maze apparatus (San Diego Instruments) and allowed to move freely for 5 min. The distance traveled and series of arm entries were recorded using video tracking software EthoVision XT 15 (Noldus). An alternation was defined as entries into all three arms on consecutive occasions. The number of maximum alternations was therefore the total number of arm entries minus two, and the percentage of alternations was calculated.

### *Barnes maze*

The Barnes maze test was conducted on a white circular surface with 20 holes equally spaced along the perimeter (Figure S6F). For acquisition trials, a shelter was placed under one of the holes, i.e. the “target hole”. Mice were placed in the center and allowed to move freely up to 3 min. The latency to reach the target, numbers of holes visited other than the target, and distance traveled were recorded using video tracking software EthoVision XT 15 (Noldus). Mice were subjected to acquisition trials twice a day for 7 d, and then to probe tests 24 h and 10 d after the last acquisition trial. In the probe tests without the shelter, mice were placed in the center and allowed to move freely for 3 min. The time spent around each hole, numbers of visiting each hole, and distance traveled were recorded. “Target zone” were defined as the target hole plus the 2 holes on either side of the target hole.

### *Contextual fear conditioning*

Conditioning and test sessions were performed in a standard operant chamber (Med Associates) equipped with a tone generator and house light. Mice were handled for habituation in front of the apparatus for 2 min per day for 3 d. On day 0, conditioning was performed (Figure S6G). Mice were placed in a test chamber inside a sound-attenuated cabinet and allowed to explore freely for 150 s. A white noise, which is conditioned stimulus, was presented for 30 s, followed by a foot shock (2 s, 1 mA) serving as unconditioned stimulus. On day 1 and 10, contextual fear memory and auditory-cued fear memory tests were performed. For the contextual fear memory test, mice were placed in the same chamber in the same context as the conditioning, and immobile time and distance traveled were recorded for 5 min. For the auditory-cued fear memory test, mice were placed in a different chamber in a different context from the conditioning. Mice were allowed to move freely for 2.5 min, and then the white noise was presented for 2.5 min. Immobile time and distance traveled were recorded automatically.

## **Quantification and statistical analyses**

Numbers of samples or animals analyzed in each experiment, statistical analysis performed, as well as *p* values for all results are described in the figure legends. For all the *in vivo* and *in vitro* experiments, “*n*” represents the number of animals and replicates, respectively. An F test, a Brown–Forsythe test, or a Bartlett's test was performed to evaluate the differences in variances. An unpaired, two-tailed Student's *t*-test, a two-tailed paired test, or a Mann–Whitney test was used to determine statistical significance between two groups. One- or two-way Analysis of Variance (ANOVA) with a Dunnett's, Tukey's, or Sidak's multiple comparison test was used to determine statistical significance among three or more groups. A linear regression model was used to test the correlation between two variables. A Fisher's exact test was

used to analyze contingency table data. Statistical calculations were performed with GraphPad Prism Software, Version 9. Differences with  $p$  values of less than 0.05 were considered significant. Statistically significant comparisons in each figure are indicated with asterisks, \* $p < 0.05$ , \*\* $p < 0.01$ , \*\*\* $p < 0.001$ , and \*\*\*\* $p < 0.0001$ . Data are presented as mean  $\pm$  SEM.

## Figures

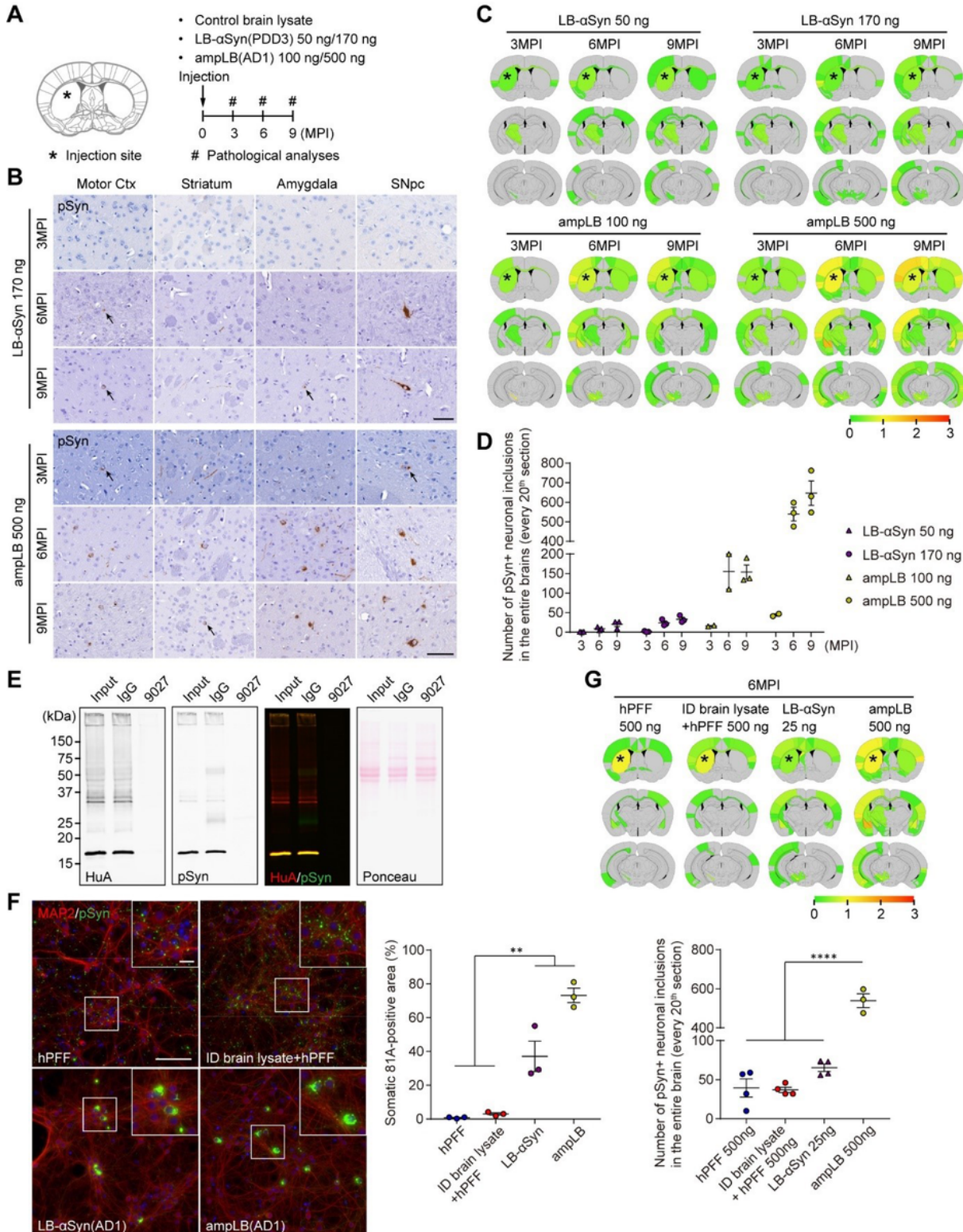


## Figure 1

**Lewy body amplification increases  $\alpha$ Syn pathology induced in WT mice.** (A) Schematic representation of experimental design. (B) Immunohistochemistry with an anti-pSyn antibody (EP1536Y). Arrows indicate pSyn-positive neuronal somatic inclusions. Motor Ctx, Motor cortex; SNpc, substantia nigra pars compacta. Scale bar 50  $\mu$ m. (C) Heat map colors represent extent of pSyn-positive pathology. (D) Number of pSyn-positive neuronal somatic inclusions in the entire brains ( $n = 2-3$  per group). (E) Western blot analysis of AD1 brain lysate immunodepleted with a control mouse IgG or an anti-human  $\alpha$ Syn antibody 9027. Immunoblots with anti-human  $\alpha$ Syn (HuA) and pSyn (81A) antibodies. (F) Left panels: Mouse primary hippocampal neurons treated with hPFF, immunodepleted (ID) AD1 brain lysate mixed with hPFF, LB- $\alpha$ Syn (AD1), and ampLB (AD1). Note that the ID brain lysate mixed with hPFF and LB- $\alpha$ Syn contain almost the same contaminants. Scale bars 100  $\mu$ m, 20  $\mu$ m (inset). Immunocytochemistry with anti-MAP2 and pSyn (81A) antibodies. Right panel: Percent of total pSyn-positive pathology in neuronal somatic inclusions ( $n = 3$  per group). One-way ANOVA with a Tukey's post-hoc test was performed;  $**p < 0.01$ . (G) Upper panel: Heat map colors represent the extent of pSyn-positive pathology at 6MPl. Lower panel: Number of pSyn-positive neuronal somatic inclusions in the entire brains ( $n = 3-4$  per group). One-way ANOVA with a Tukey's post-hoc test was performed;  $****p < 0.0001$ . Data are represented as mean  $\pm$  SEM.

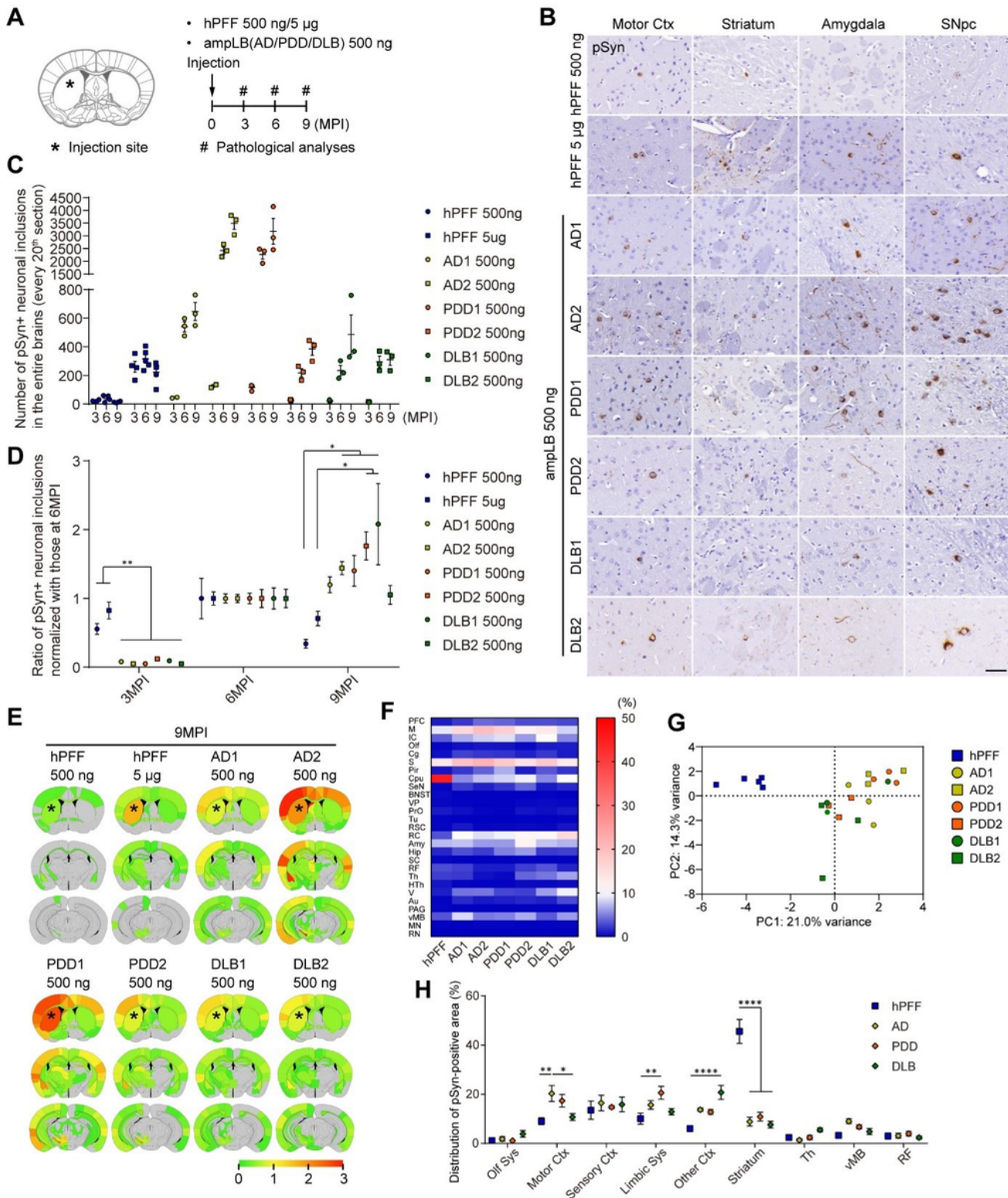


**Figure 2**

**Differences in seeding activity and distribution of  $\alpha$ Syn pathology between hPFF and ampLB in WT mice.**

(A) Schematic representation of experimental design. (B) Immunohistochemistry with an anti-pSyn antibody (EP1536Y) at 6MPI. Motor Ctx, motor cortex; SNpc, substantia nigra pars compacta. Scale bar 50  $\mu$ m. (C) Number of pSyn-positive neuronal somatic inclusions in the entire brains ( $n = 2-5$  per group). (D) Ratio of numbers of pSyn-positive neuronal somatic inclusions normalized with those at 6MPI ( $n =$



2–5 per group). One-way ANOVA with a Tukey's post-hoc test was performed for 3MPI and 9MPI; \* $p < 0.05$  and \*\* $p < 0.01$ . (E) Heat map colors represent the extent of pSyn-positive pathology at 9MPI. (F) Heat map colors represent proportion of pSyn-positive area in each brain region shown in Figure S5B at 9MPI. (G) Primary component analysis of the distribution of pSyn-positive pathology at 9MPI. (H) Distribution of pSyn-positive pathology in the brain systems at 9MPI (n = 5–6 per group). Olf Sys, olfactory system; Motor Ctx, motor cortex; Sensory Ctx, sensory cortex; Limbic Sys, limbic system; Th, thalamus; vMB, ventral midbrain; RF, reticular formation. Two-way ANOVA with a Sidak's post-hoc test was performed; interaction ( $p < 0.0001$ ), \* $p < 0.05$ , \*\* $p < 0.01$ , and \*\*\*\* $p < 0.0001$ . Data are represented as mean  $\pm$  SEM.

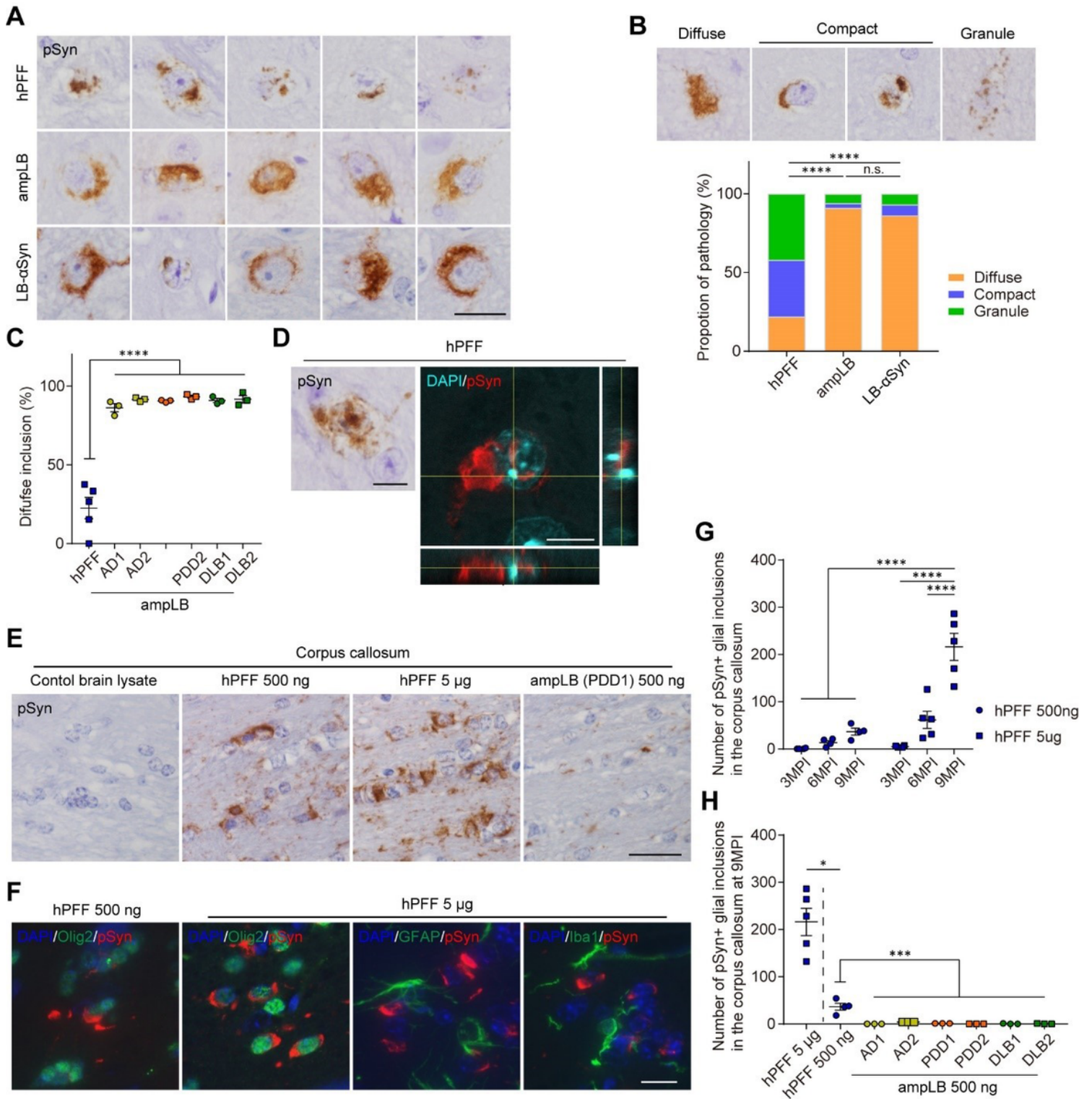


**Figure 3**

**Differences in morphology of neuronal inclusions and cell-type preference between hPFF and ampLB in WT mice.** (A) High-magnification images of pSyn-positive neuronal inclusions in the SN of hPFF-, ampLB-, and LB- $\alpha$ Syn-injected mice at 6MPl. Scale bar 20  $\mu$ m. (B) Upper panels: Representative images of diffuse, compact, and granular pSyn-positive inclusions. Lower panels: Comparison of the proportions of diffuse, compact, and granular inclusions (hPFF, n = 50; ampLB, n = 959; LB- $\alpha$ Syn, n = 29). A Fisher's

exact test was performed between two groups for differences in the percentages of diffuse and non-diffuse inclusions; \*\*\*\* $p < 0.0001$ , n.s., not significant. (C) Percent of diffuse inclusions in hPFF- and ampLB-injected mice ( $n = 3-5$  per group). One-way ANOVA with a Tukey's post-hoc test was performed; \*\*\*\* $p < 0.0001$ . (D) Immunohistochemistry and z-stack confocal microscopy images showing pSyn-positive intranuclear inclusions in hPFF-injected mice. Scale bars 10  $\mu\text{m}$ . (E) Immunohistochemistry with a pSyn antibody (EP1536Y) in the corpus callosum at 9MPI. (F) Double immunofluorescence for Olig2 (green) and pSyn (81A, red), GFAP (green) and pSyn (EP1536Y, red), and Iba1 (green) and pSyn (81A, red). (G) Number of pSyn-positive oligodendroglial inclusions in the corpus callosum ( $n = 4-5$  per group). Two-way ANOVA with a Sidak's post-hoc test was performed; interaction ( $p = 0.0001$ ), \*\*\*\* $p < 0.0001$ . (H) Number of pSyn-positive oligodendroglial inclusions in the corpus callosum at 9MPI ( $n = 3-5$  per group). A Mann Whitney test was performed between hPFF 5  $\mu\text{g}$  and hPFF 500 ng; \* $p < 0.05$ . One-way ANOVA with a Tukey's post-hoc test was performed among hPFF 500 ng and ampLB preparations; \*\*\* $p < 0.001$ . Data are represented as mean  $\pm$  SEM.

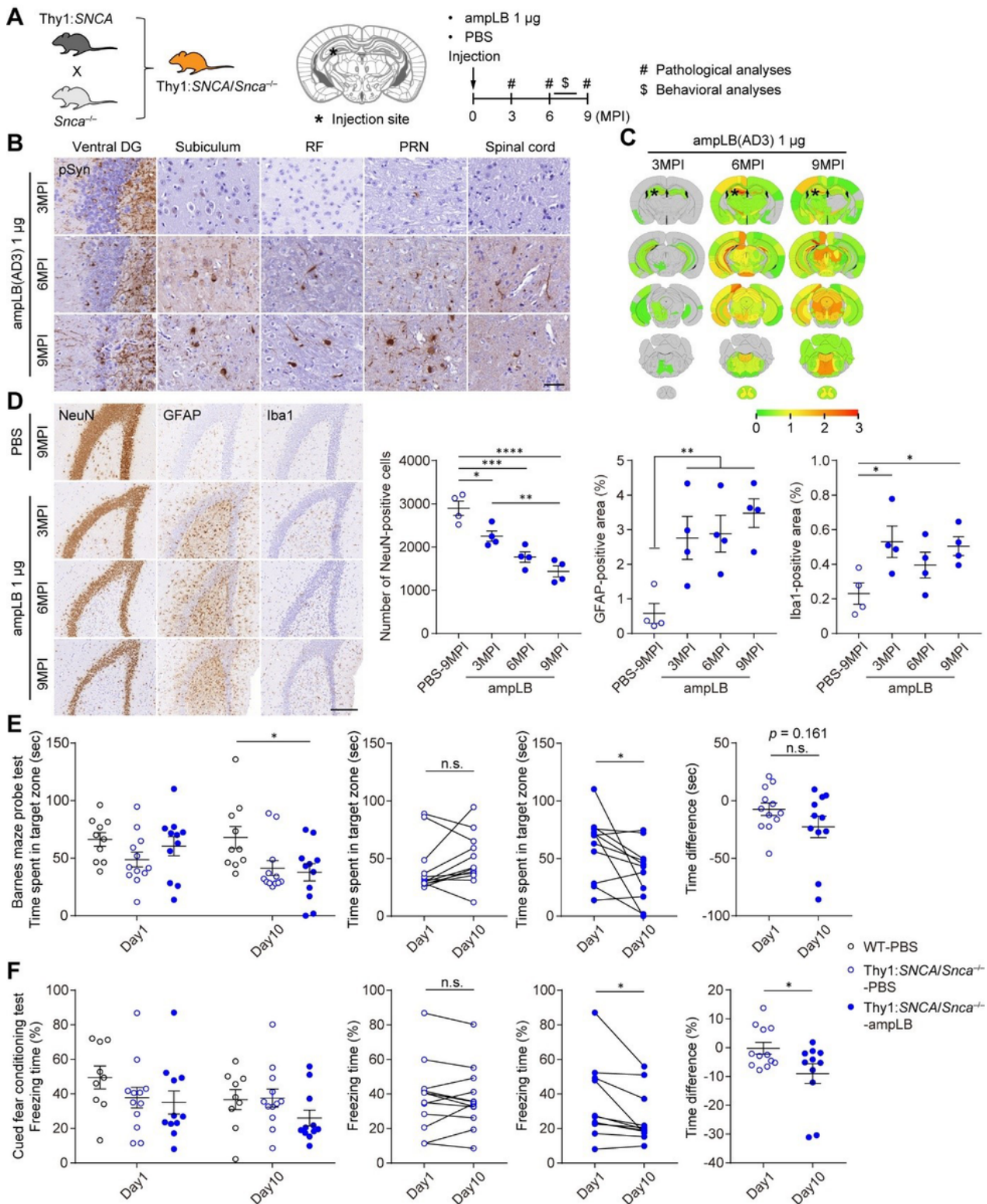


**Figure 4**

**Modeling LBD in Thy1:SNCA/Snca<sup>-/-</sup> mice.** (A) Schematic representation of experimental design. (B) Immunohistochemistry with an anti-pSyn antibody (EP1536Y) on the ipsilateral side. Ventral DG, ventral dentate gyrus; RF, reticular formation; PRN, pontine reticular formation. Scale bar 50 µm. (C) Heat map colors represent extent of pSyn-positive pathology. (D) Left panels: Immunohistochemistry with anti-NeuN, GFAP, and Iba1 antibodies in the ipsilateral ventral dentate gyrus. Scale bar 200 µm. Right panels:



Number of NeuN-positive cells, GFAP-positive area, and Iba1-positive area in the ipsilateral ventral dentate gyrus ( $n = 4$  per group). One-way ANOVA with a Tukey's post-hoc test was performed for number of NeuN-positive cells and GFAP-positive area. One-way ANOVA with a Dunnett's post-hoc test was performed for Iba1-positive area;  $*p < 0.05$ ,  $**p < 0.01$ ,  $***p < 0.001$ , and  $****p < 0.0001$ . (E) Barnes maze probe test at 7MPI ( $n = 10-12$  per group). Left panel: Time spent in a target zone at day1 and day10. One-way ANOVA with a Tukey's post-hoc test was performed for day10;  $*p < 0.05$ . Middle panels: Time spent in a target zone between day1 and day10. A two-tailed paired test was performed;  $*p < 0.05$ , n.s., not significant. Right panel: Difference in time spent in a target zone between day1 and day10. A two-tailed unpaired Student's  $t$ -test was performed; n.s., not significant. (F) Cued fear conditioning test at 8MPI ( $n = 9-12$  per group). Left panel: Freezing time during auditory cue at day1 and day10. Middle panels: freezing time between day1 and day10. A two-tailed paired test was performed;  $*p < 0.05$ , n.s., not significant. Right panel: Difference in freezing time between day1 and day10. A two-tailed unpaired Student's  $t$ -test was performed;  $*p < 0.05$ . Data are represented as mean  $\pm$  SEM.

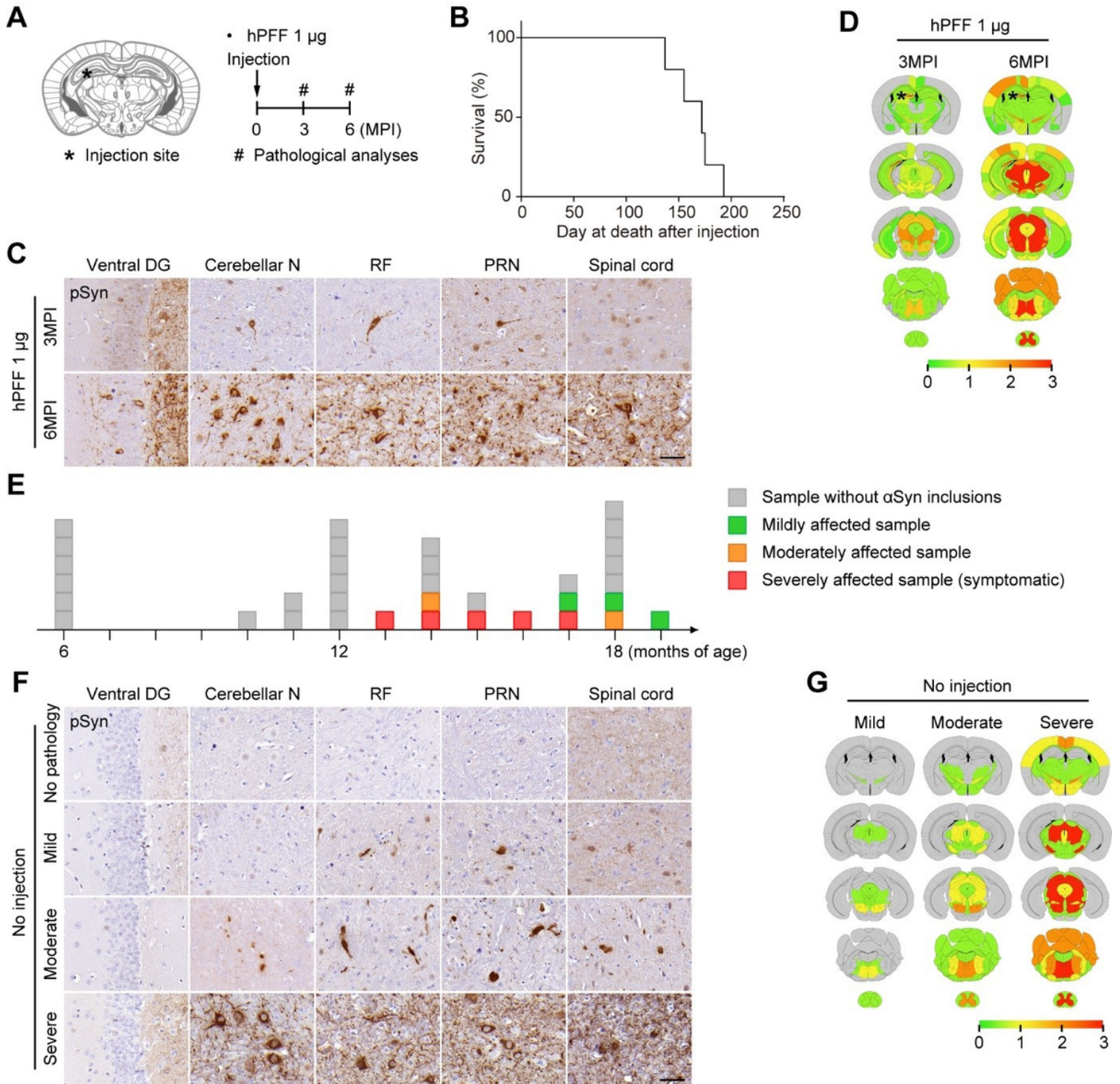


**Figure 5**

**hPFF injection into *Thy1:SNCA/Snca*<sup>-/-</sup> mice induces pathological and phenotypic features distinct from ampLB.** (A) Schematic representation of experimental design. (B) Survival curve of hPFF-injected

*Thy1:SNCA/Snca*<sup>-/-</sup> mice (n = 5). (C) Immunohistochemistry with an anti-pSyn antibody EP1536Y on the ipsilateral side. Ventral DG, ventral dentate gyrus; Cerebellar N, cerebellar nuclei; RF, reticular formation; PRN, pontine reticular nucleus. Scale bar 50 µm. (D) Heat map colors represent extent of pSyn-positive pathology. (E) Schematic representation of age and severity of  $\alpha$ Syn pathology. Each box represents one



Thy1:*SNCA/Snca*<sup>-/-</sup> mouse. Color indicates severity of αSyn pathology (gray, sample without αSyn inclusions; green, mildly affected sample; orange, moderately affected sample; red, severely affected sample). (F) Immunohistochemistry with an anti-pSyn antibody EP1536Y on the ipsilateral side. Arrows indicate pSyn-positive inclusions. Scale bar 50 μm. (G) Heat map colors represent extent of pSyn-positive pathology.

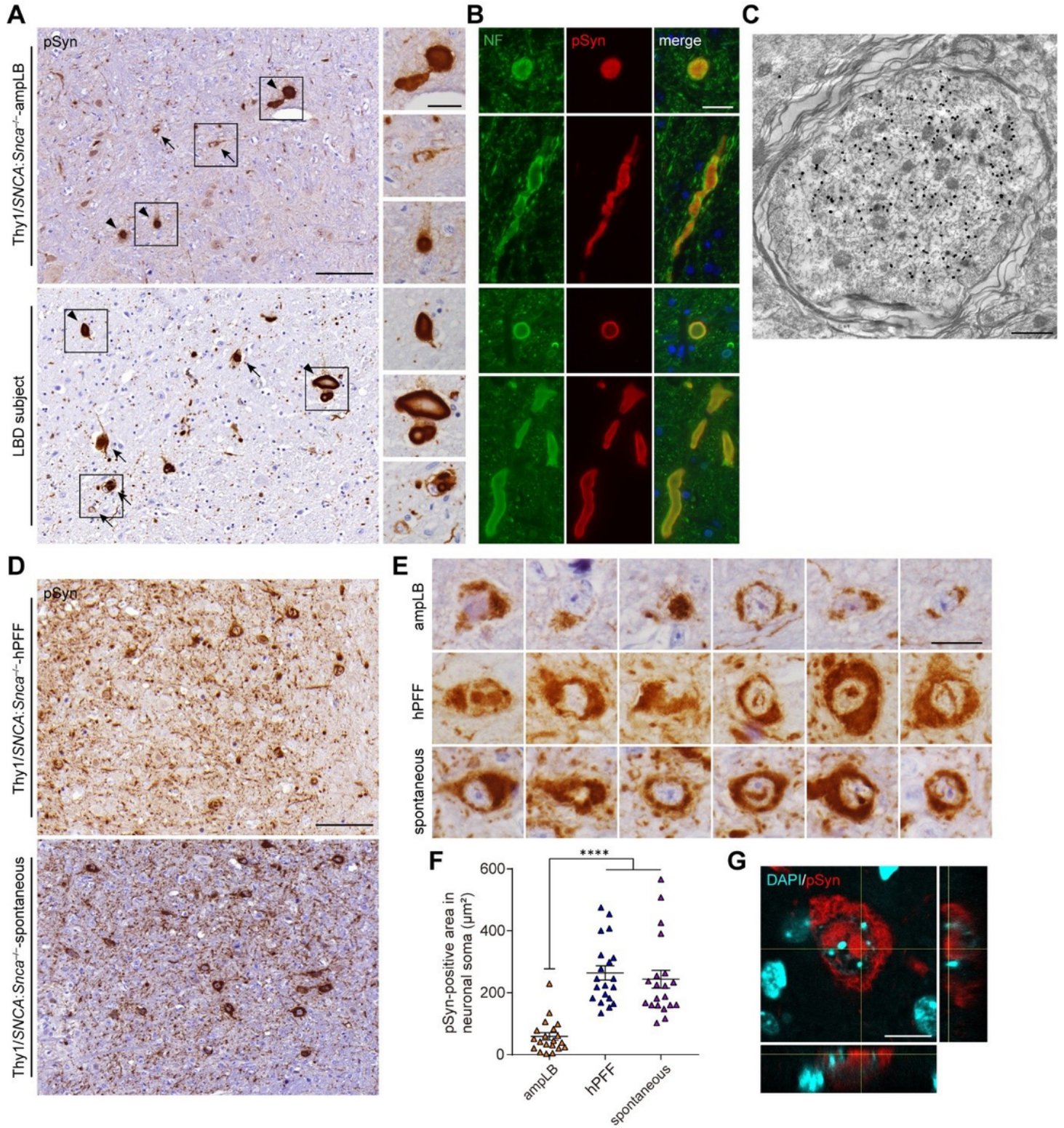
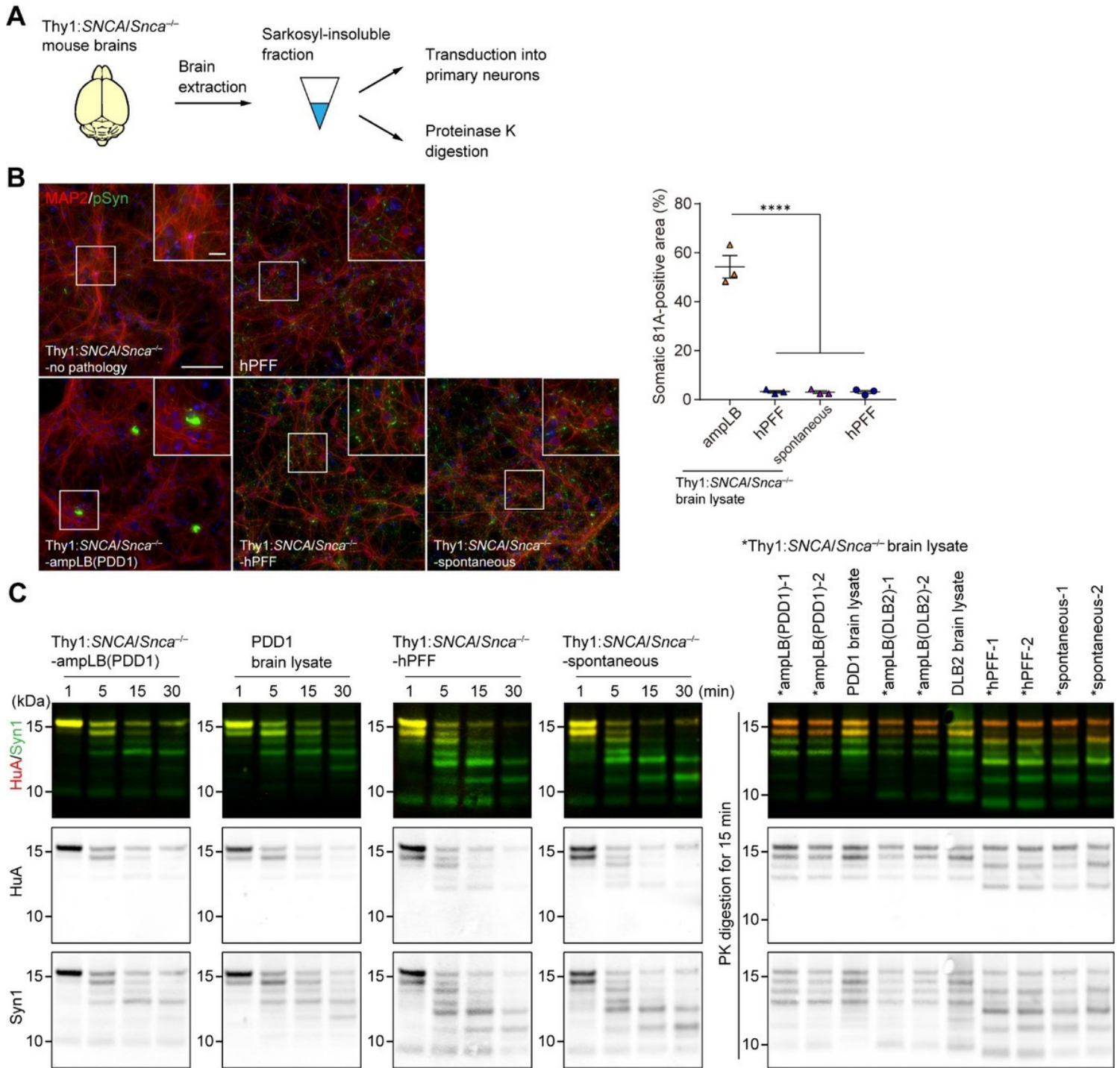


Figure 6

**Similarities and differences in pathological characteristics among Thy1:*SNCA/Snca*<sup>-/-</sup> mouse models and LBD subjects.** (A) Immunohistochemistry with an anti-pSyn antibody (EP1536Y) in the pons of an ampLB-injected Thy1:*SNCA/Snca*<sup>-/-</sup> mouse (Thy1:*SNCA/Snca*<sup>-/-</sup>-ampLB) at 9MPI and a LBD subject. Arrows and arrowheads indicate pSyn-positive neuronal inclusions and axonal swelling-like structures, respectively. Scale bars 100  $\mu$ m, 20  $\mu$ m (inset). (B) Double immunofluorescence for neurofilament (NF, green) and pSyn (#64, red). Upper panels: an ampLB-injected Thy1:*SNCA/Snca*<sup>-/-</sup> mouse, Lower panels: a LBD subject. Scale bar 20  $\mu$ m. (C) Immunoelectron micrograph of an axonal swelling in the pons of an ampLB-injected Thy1:*SNCA/Snca*<sup>-/-</sup> mouse with immunogold-labeled pSyn (EP1536Y). Scale bar 1  $\mu$ m. (D) Immunohistochemistry with an anti-pSyn antibody EP1536Y in the pons of a hPFF-injected Thy1:*SNCA/Snca*<sup>-/-</sup> mouse (Thy1:*SNCA/Snca*<sup>-/-</sup>-hPFF) at 6MPI and a Thy1:*SNCA/Snca*<sup>-/-</sup> mouse with spontaneous  $\alpha$ Syn pathology (Thy1:*SNCA/Snca*<sup>-/-</sup>-spontaneous) at 13 months of age. (E) High-magnification images of pSyn-positive neuronal inclusions in the pons of ampLB-injected Thy1:*SNCA/Snca*<sup>-/-</sup> mice at 6MPI, hPFF-injected Thy1:*SNCA/Snca*<sup>-/-</sup> mice at 6MPI, and Thy1:*SNCA/Snca*<sup>-/-</sup> mice with spontaneous  $\alpha$ Syn pathology. Scale bar 20  $\mu$ m. (F) PSyn-positive area in neuronal soma (n = 20 per group). One-way ANOVA with a Tukey's post-hoc test was performed; \*\*\*\* $p < 0.0001$ . (G) Z-stack confocal microscopy images showing pSyn-positive intranuclear inclusions in hPFF-injected mice. Scale bar 10  $\mu$ m. Data are represented as mean  $\pm$  SEM.





**Figure 7**

**AmpLB-induced pathological  $\alpha$ Syn in Thy1:*SNCA/Snca*<sup>-/-</sup> mice maintains the biological and conformational features of original LB- $\alpha$ Syn.** (A) Schematic representation of experimental design. (B) Left panels: Mouse primary hippocampal neurons treated with brain lysates of Thy1:*SNCA/Snca*<sup>-/-</sup> mice without  $\alpha$ Syn pathology (Thy1:*SNCA/Snca*<sup>-/-</sup>-no pathology), ampLB-injected Thy1:*SNCA/Snca*<sup>-/-</sup> mice (Thy1:*SNCA/Snca*<sup>-/-</sup>-ampLB), hPFF-injected Thy1:*SNCA/Snca*<sup>-/-</sup> mice (Thy1:*SNCA/Snca*<sup>-/-</sup>-hPFF), and old Thy1:*SNCA/Snca*<sup>-/-</sup> mice with spontaneous  $\alpha$ Syn pathology (Thy1:*SNCA/Snca*<sup>-/-</sup>-spontaneous), and hPFF. Immunocytochemistry with MAP2 and pSyn (81A) antibodies. Scale bars 100  $\mu$ m, 20  $\mu$ m (inset).

Right panel: Percent of total pSyn-positive pathology in somatic inclusions (n = 3 per group). One-way ANOVA with a Tukey's post-hoc test was performed; \*\*\*\* $p < 0.0001$ . Scale bar 10  $\mu\text{m}$ . (C) Proteinase K (PK) digestion on Thy1:*SNCA*/*Snca*<sup>-/-</sup> mouse brain lysate and LBD brain lysate. Left panels: Samples were subjected to PK digestion for 1, 5, 15, and 30 min, followed by western blot analysis with anti-human  $\alpha\text{Syn}$  antibodies HuA and Syn1. Right panel: Samples were subjected to PK digestion for 15 min, followed by western blot analysis with HuA and Syn1 antibodies. Data are represented as mean  $\pm$  SEM.

## Supplementary Files

This is a list of supplementary files associated with this preprint. Click to download.

- [MovieS1.mp4](#)
- [SupplementaryInformation.docx](#)